Certain Optics Considerations for the Holography Experiment

Xiaolei Zhang

November 7, 1996

Submillimeter Array Memorandum, No. 86

Original Version: June 14, 1995

Abstract

This memo addresses several optics-related issues for the upcoming SMA holography experiment[1]. These issues include: (a) the establishment of a Fourier transform relation between the measured far-field radiation pattern and the sought-for aperture phase-error distribution; (b) the effect and the correction for the secondary mirror diffraction; (c) the determination of the size of the feed of the main receiver to achieve a certain illumination taper; (d) the determination of the size of the reference feed so as to maintain nearly constant amplitude and phase over the entire range of angular scan of the far-field measurement; (e) the choice of location for the main receiver feed along the antenna's optical axis, which takes into account the fact that the subreflector is not yet at the far field of the main receiver feed; (f) the determination of the phase reference plane, and the calculation of the accuracy needed for determining the distances from the reference feed as well as from the antenna aperture to the intersecting point of the azimuth and elevation axes; (g) the near-field effect introduced by the local transmitter and its partial correction, as well as the estimation of the accuracy needed for determining the distance to the transmitter; (h) the calculation of the amount of subreflector movement needed to focus the antenna at 250 m distance. (e) the estimation of the effect of aliasing for the number of sample points we choose to use. In the Appendices, we also include discussions of the the procedures used for designing the dielectric lenses used at the apertures of the feeds; as well as the calculations of the phase errors introduced due to a unit length of subreflector and feed movement. A summary of the relevant measurement accuracies needed in order to achieve a surface rms on the order of 5 μm is as follows: The measurement of the distance from the antenna pivoting point to the transmitter should be accurate to about 14 cm; The distances from the the reference feed and from the antenna aperture to the pivoting point should be known to better than 15 mm each.

[1]The detailed description of the general requirement, as well as the hardware and software preparation for the holography experiment can be found in the SMA technical memo No. 85 by Zhang et al. (1995).

1 Derivation of the Fourier Transform Relation

Following the formulation of Rahmat-Samii (1984), in Figure 1 we plot a paraboloid of diameter D and focal length F. In the discussion of this section we assume that the phase reference center is at the primary focus, which corresponds to the effective pivoting point we discuss later. It is a well-known result from physical optics that the far field radiation pattern of such a reflector is

$$\vec{E} = -jk\eta \frac{e^{-jkr}}{4\pi r}(T_\theta \hat{\theta} + T_\phi \hat{\phi}), \tag{1}$$

where k is the wave number, $\eta = 120\pi$ is the free space impedance, and

$$\vec{T}(\theta, \phi) = \int_S \vec{J} e^{jk\vec{r}' \cdot \hat{r}} dS' \tag{2}$$

where $\vec{J}$ is the induced current on the paraboloid, which is related to the incident magnetic field $\vec{H}^i$ by

$$\vec{J} = 2\hat{n} \times \vec{H}^i \tag{3}$$

where $\hat{n}$ is the normal vector of the surface S.

We can further express the integral (2), using the aperture coordinate (x', y'), as

$$\vec{T}(\theta, \phi) = \int_S \vec{J}(\vec{r}') e^{jk\vec{r}' \cdot \hat{r}} \left[1 + (\frac{\partial f}{\partial x'})^2 + (\frac{\partial f}{\partial y'})^2\right]^{1/2} dx' dy', \tag{4}$$

where $f(x, y) = z$ is the reflector surface-profile function.

Now define

$$\check{J}(x', y') = \vec{J}(\vec{r}') \left[1 + (\frac{\partial f}{\partial x'})^2 + (\frac{\partial f}{\partial y'})^2\right]^{1/2}, \tag{5}$$

and use also

$$\vec{r}' \cdot \hat{r} = z' \cos\theta + ux' + vy' \tag{6}$$

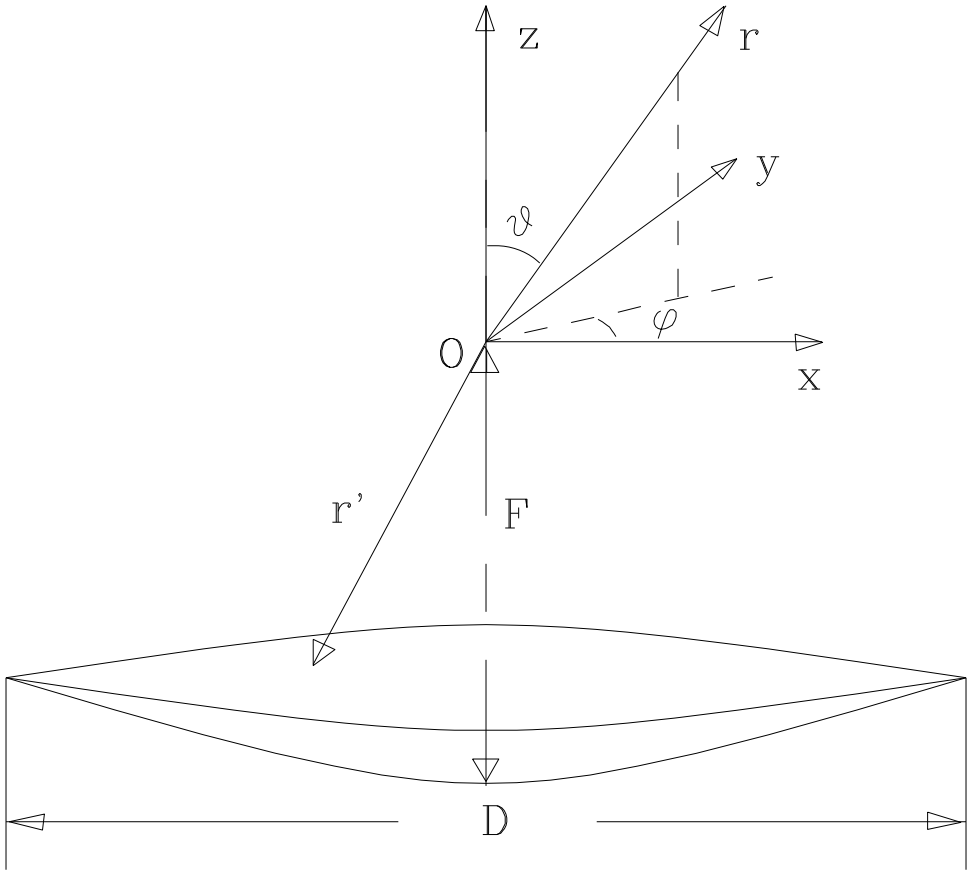

Figure 1: Geometry of the primary paraboloid reflector and the coordinate system

where

$$u = \sin\theta\cos\phi, \qquad v = \sin\theta\sin\phi \tag{7}$$

we obtain

$$\vec{T}(u,v) = \int_S \tilde{J}(x',y')e^{jkz'}e^{jk(ux'+vy')}dx'dy' \tag{8}$$

where we have assumed $\cos\theta \approx 1$ for the range of far-field scanning angle we are interested.

It can be shown that if the electric field at the feed aperture is predominantly y-polarized, then for small θ range the copolar component of the far-field pattern $T_{copolar} \approx T_y$, and the cross-polar component $T_{cross-polar} \approx T_x$. Therefore considering the copolar component only we can write (8) in the form of a scalar equation

$$T(u,v) = \int_S |\tilde{J}(x',y')|e^{-jkr'+jkz'}e^{jk(ux'+vy')}dx'dy', \tag{9}$$

where we have made use of the fact that the phase center is chosen to be at the primary focus, and where $|\tilde{J}(x',y')|$ is the magnitude of the effective current on the aperture plane.

Having arrived at the relation between the far-field pattern and the surface-current distribution (9), we now try to derive the expression for the surface error distribution.

In Figure 2, assuming that $\epsilon(x,y)$ is the distribution of surface error in the direction normal to the surface, we have that for small distortion

$$\begin{aligned} P'P + PQ &= \frac{\epsilon}{\cos\xi} + \frac{\epsilon}{\cos\xi}\cos 2\xi \\ &= 2\epsilon\cos\xi, \end{aligned} \tag{10}$$

where we know from the equation of a paraboloid,

$$\cos\xi = (1 + \frac{\rho^2}{4F^2})^{-1/2} = (1 + \frac{x^2+y^2}{4F^2})^{-1/2}. \tag{11}$$

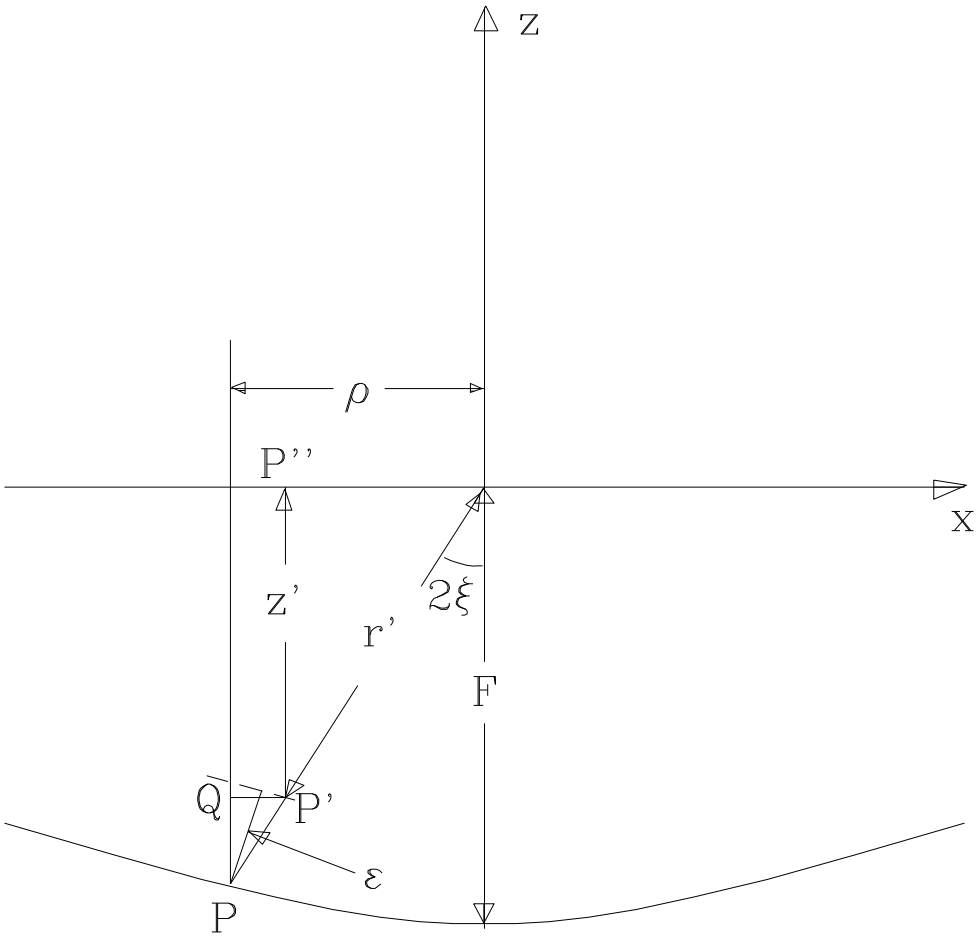

Figure 2: Geometry for calculating the surface distortion

We now find that

$$\begin{aligned} -r' + z' &= -r' - P'P" \\ &= -r' - P'P" - P'P - PQ + P'P + PQ \\ &= -2F + 2\epsilon\cos\xi \end{aligned} \tag{12}$$

Define the total distortion phase error

$$\delta = 4\pi(\epsilon/\lambda)\cos\xi \tag{13}$$

equation (9) becomes

$$T(u,v) = e^{-j2kF}\int_S |\tilde{J}(x',y')|e^{j\delta}e^{jk(ux'+vy')}dx'dy' \tag{14}$$

Therefore we finally obtain the Fourier transform relation

$$|\tilde{J}(x,y)|e^{j\delta} = e^{j2kF}\mathcal{F}[T(u,v)] \tag{15}$$

or

$$\frac{\epsilon(x,y)}{\lambda} = \frac{1}{4\pi}(1+\frac{x^2+y^2}{4F^2})^{1/2}\text{phase}\{e^{j2kF}\mathcal{F}[T(u,v)]\} \tag{16}$$

Note that here the convention for the Fourier transform used is such that the forward transform has the minus signs on the exponential.

2 Secondary Mirror Diffraction

The formulation in this section follows largely the unpublished notes of Richard Hills.

It is easier to estimate the effect of secondary mirror diffraction when the antenna is in the transmitting mode. The diffraction pattern obtained should be identical to that in the receiving mode from the reciprocity theorem.

The major effect of secondary mirror diffraction is the ripples it causes in the amplitude and phase of the primary illumination pattern. There is also a second diffraction effect, caused by the signal from the feed which passes directly the edge of the secondary mirror, which leads to the formation of a Poisson spot in the boresight direction. Since this second diffraction effect is smaller (it is down by a factor of *Gain(primary)/Gain(secondary)/Edge-Taper*, which is about 35 dB compared to the intensity due to the signal which has passed through the Cassegrain system, at the boresight direction), and more difficult to correct, we will here consider only the first diffraction effect.

In Figure 3(a), assuming a point source at O illuminates an open screen (aperture) S. It is assumed that the light outside S is block by a dark screen. The field at P due to the influence of the illuminated screen S can be calculated by the Kirchhoff diffraction integral

$$E(P) = \frac{-i}{2\lambda} \int_S \frac{A(S) e^{-ik(r+r')}}{rr'} (\cos\theta_i + \cos\theta_0) dS. \tag{17}$$

For the actual geometry of an Cassegrain antenna (Figure 3b), the Kirchhoff integral becomes

$$E(P) = \frac{-iA_0}{2\lambda} \int_{secondary} \frac{e^{-(\frac{r}{r_t})^2} e^{-ik(ps+pp)}}{ps \cdot pp} (\cos\theta_i + \cos\theta_0) dS, \tag{18}$$

where we have assumed that the illumination pattern from the feed is a Gaussian, with characteristic radius which relates to the secondary edge taper $Taper(dB)$ and the secondary radius R_s through

$$R_t = \frac{R_s}{\sqrt{Taper(dB)/20 \cdot \ln 10}}. \tag{19}$$

We now need to calculate the different factors in the Kirchhoff integral. Assume origin O is half way in between the two foci, the equation of the secondary is (assuming r is the horizontal distance and z is the vertical distance from origin for a point on the secondary surface)

(a) Kirchhoff's integral

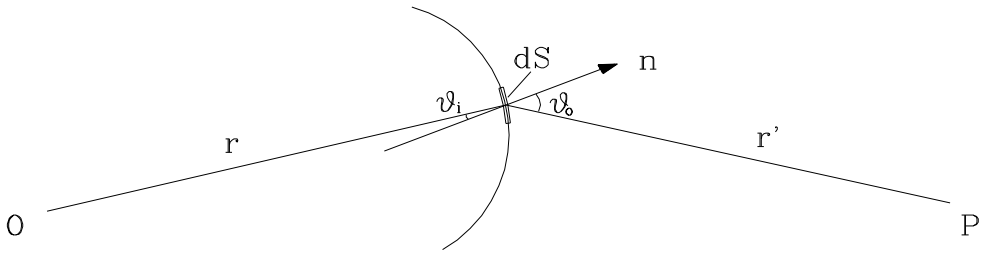

(b) Secondary mirror diffraction

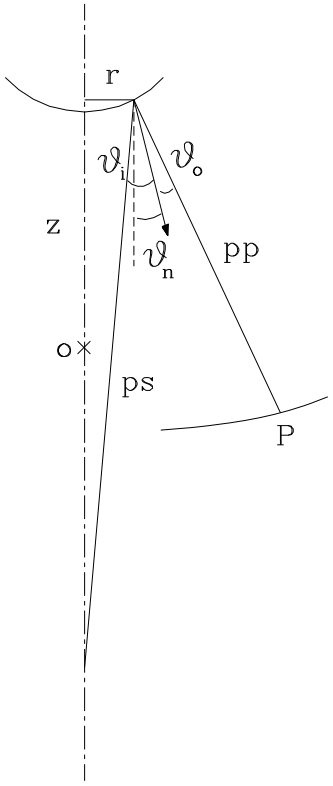

Figure 3: Secondary mirror diffraction calculation

$$\frac{z^2}{a^2} - \frac{r^2}{a^2(e^2-1)} = 1 \tag{20}$$

where $a = c/e$, with c equal to one half the inter-focal distance and e equal to the eccentricity of the secondary.

Therefore the solution for z becomes

$$z = (a^2 + \frac{r^2}{e^2-1})^{1/2} \tag{21}$$

Differentiate it, we obtain

$$\frac{dz}{dr} = \frac{r}{z(e^2-1)} \tag{22}$$

Therefore

$$\theta_n = \tan^{-1}\left[\frac{r}{z(e^2-1)}\right] \tag{23}$$

where θ_n is the angle between the normal to the secondary surface and the vertical direction.

Now we try to get the expressions for the cosine factors. Referring to Figure 3 (b), and remembering that the optical path drawn there is for the aid of diffraction calculation, which in general does not correspond to an actual ray path in geometrical optics

$$\cos\theta_i = \cos(\theta_s + \theta_n) = \cos\theta_s \cos\theta_n - \sin\theta_s \sin\theta_n \tag{24}$$

with

$$\sin\theta_s = \frac{r}{ps} = \frac{r}{\sqrt{r^2 + (c+z)^2}} \tag{25}$$

and

$$\cos\theta_s = \frac{z+c}{ps} \tag{26}$$

$$\cos\theta_0 = \hat{n}\cdot\hat{pp}. \tag{27}$$

Finally, the equation of the primary in the vertex-centered coordinates is

$$z_p = \frac{r_p^2}{4F}. \tag{28}$$

The calculated one dimensional amplitude and phase illumination pattern on the primary, for SMA geometry and for 11.2 dB edge taper is given in Figure 4 and Figure 5. Figure 6 gives the two-dimensional phase diffraction map. Note that the four-fold symmetry observed on the pattern is NOT due to the inclusion of quadrupod diffraction. Rather it is the result of interference of the rectangular plotting grid with the circular rings on the diffraction pattern.

3 Determination of the Sizes of the Feeds – Far-Field Calculations

3.1 The Size of the Main Holography Feed

In the initial holography test at the Haystack site, we choose to place the main holography feed on the optical axis near the Cassegrain focus. We first decide the size of the feed using far field calculations. The near-field effect due to that the subreflector is not yet at the far feed of the main feed, which mainly influences the location of the feed on the optical axis and the actual edge taper obtained on the secondary, is calculated in the next section.

We choose to use a phase-corrector lens on the aperture of the feed so that the wavefront curvature is zero right in front of the lens[2], to match the wave front cur-

[2]In reality the flat-curvature image is formed a little into the depth of the lens for a thick lens.

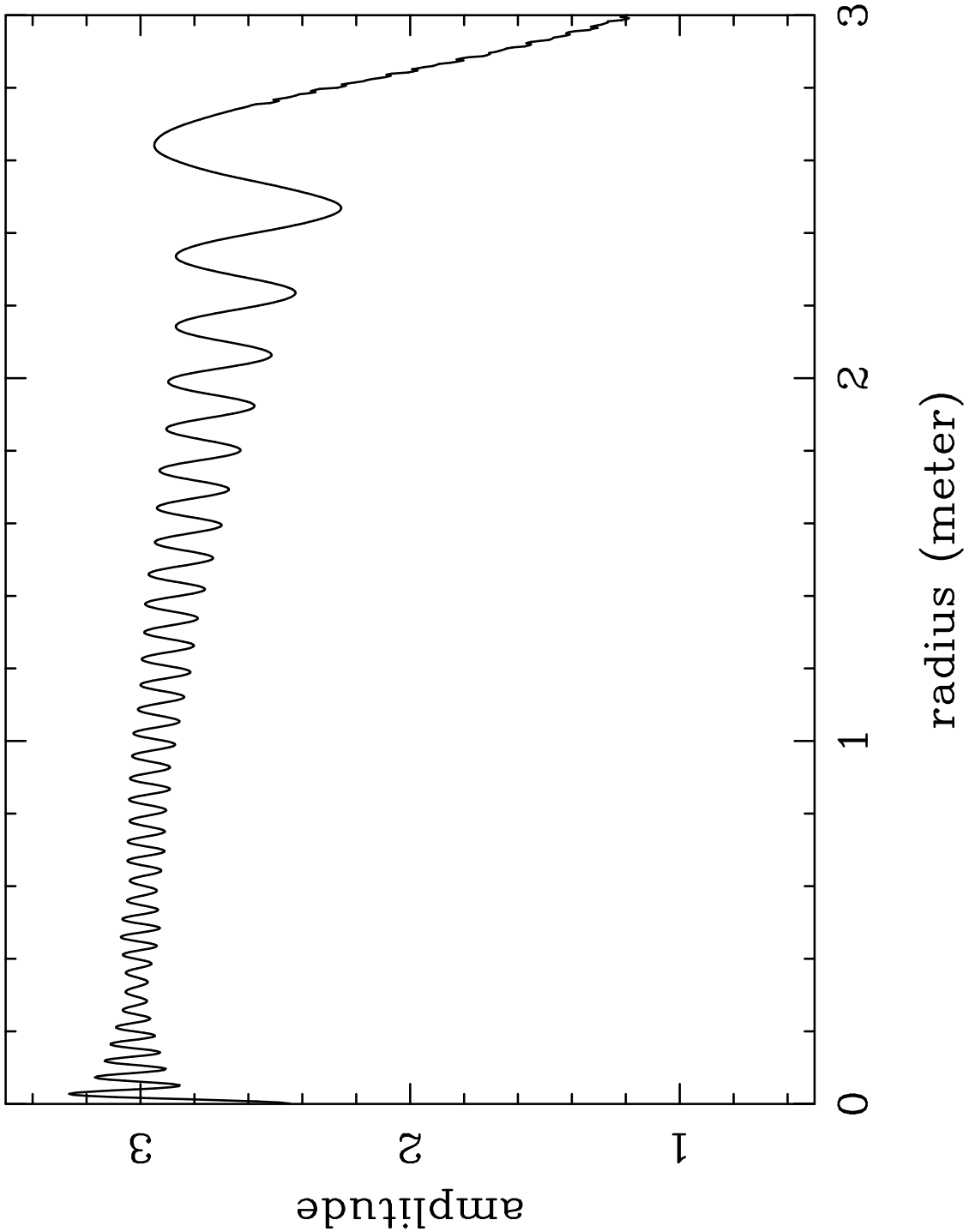

Figure 4: Amplitude profile of the secondary mirror diffraction pattern

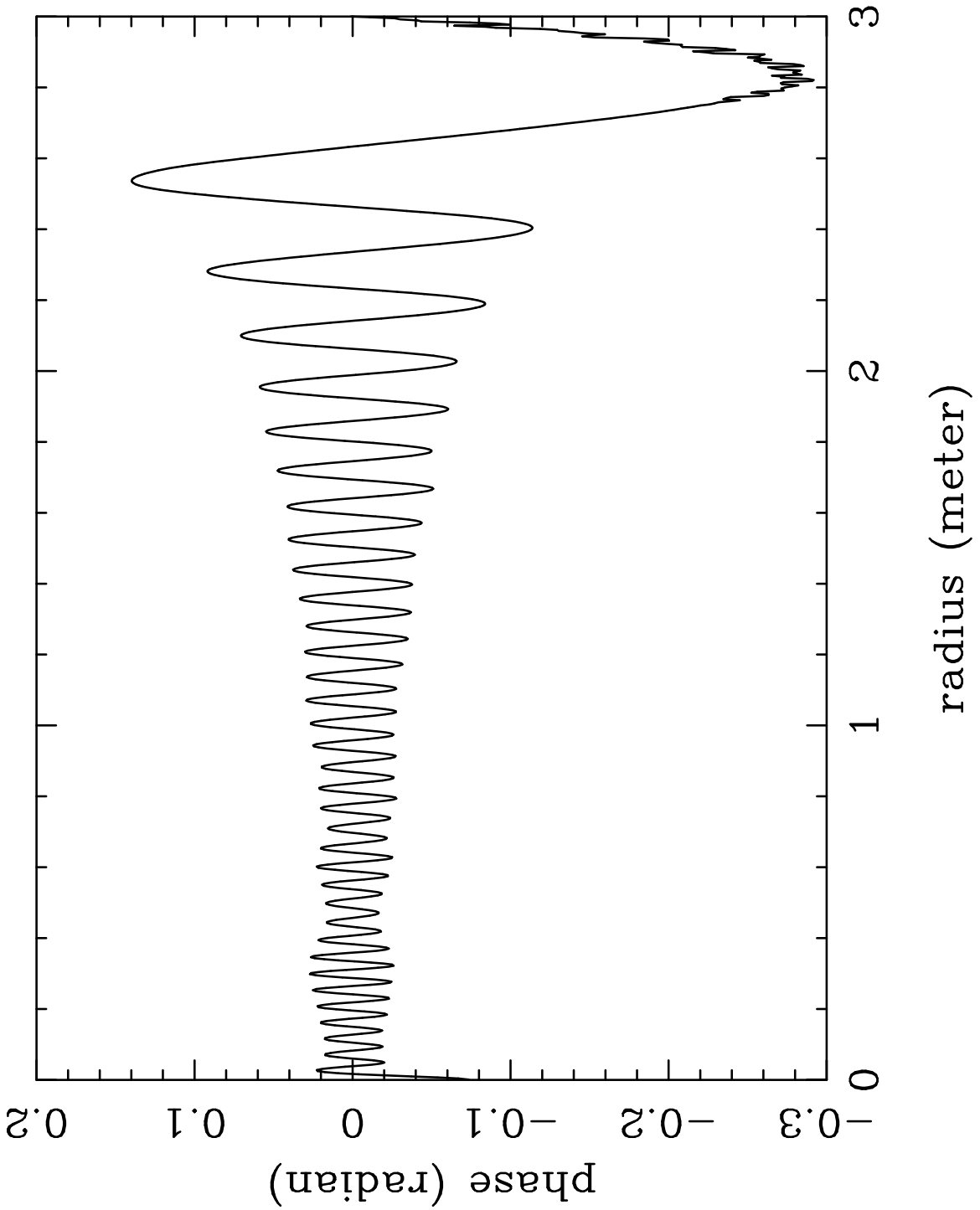

Figure 5: Phase profile (in radian) of the secondary mirror diffraction pattern

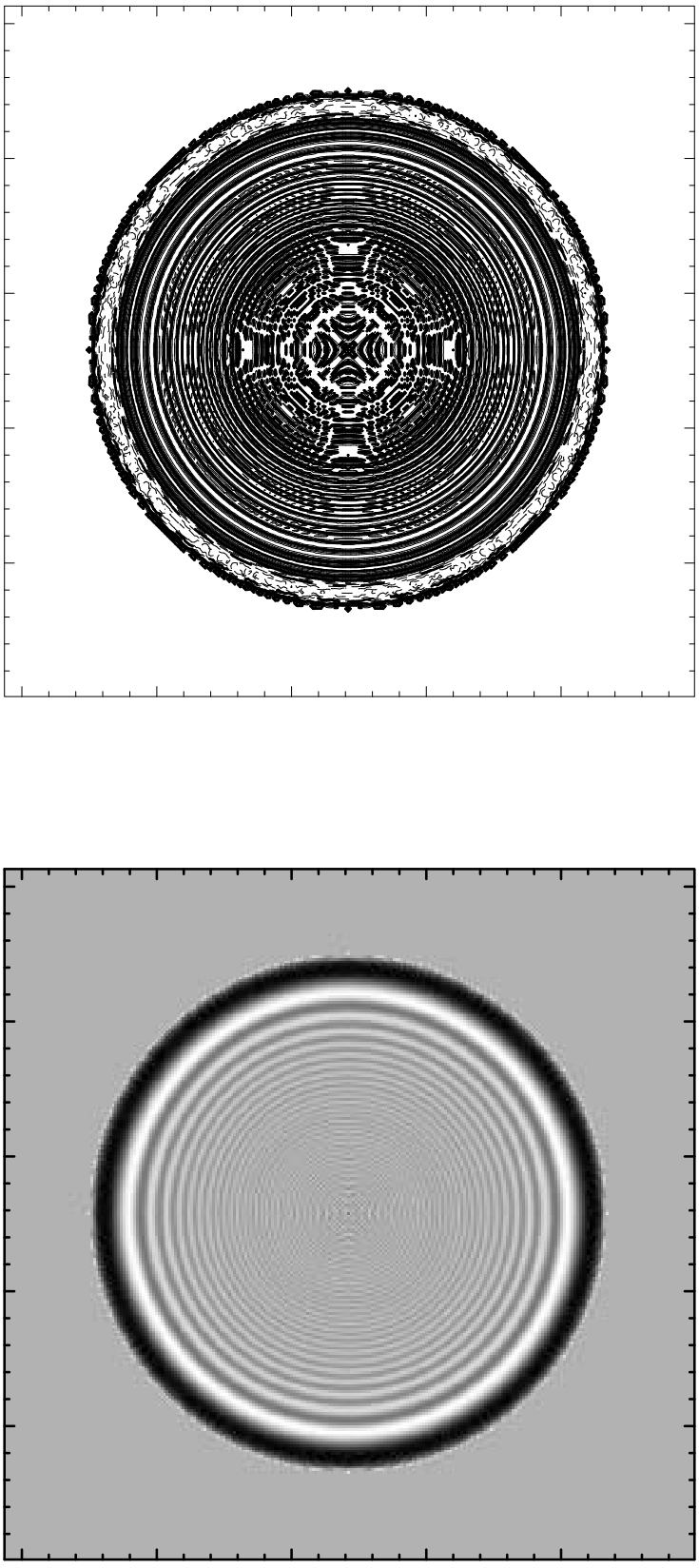

Figure 6: Two dimensional map of the diffraction pattern in phase

vature of the incoming field at the Cassegrain focus. The design procedure for such a phase-corrector lens is given in the appendix.

The far-field radiation pattern of a scalar feed with a phase corrector lens is given by (Dragone 1977)

$$\vec{F} = N_0(u,v)\hat{i_x} + \frac{\gamma-1}{\gamma+1}N_2(u,v)(\cos 2\phi\hat{i_x} + \sin 2\phi\hat{i_y}), \tag{29}$$

where

$$u = 2.4048 \tag{30}$$

$$v = ka\sin\theta \tag{31}$$

and

$$N_k(u,v) = \frac{a^2}{v^2-u^2}[vJ_k(u)J_1(v) - uJ_k(v)J_1(u)]. \tag{32}$$

In the above equations, a is the (equivalent) aperture radius of the feed, here we say "equivalent" since the thick lens effectively magnifies the size of the feed by about 4%, and the a in the about expressions takes into account of this magnification.

Our feed uses the balanced mode, (Zhang 1993), so $\gamma = 1$. Therefore the far-field pattern is

$$\begin{aligned}\vec{F} &= N_0(u,v)\hat{i_x} \\ &= \frac{a^2}{v^2-u^2}[vJ_0(u)J_1(v) - uJ_0(v)J_1(u)]\hat{i_x}\end{aligned} \tag{33}$$

If we choose the edge taper to be around 10 dB, and also make use of the fact that the half-angle that the subreflector subtends from the Cassegrain focus is $\theta = 2.046^o$, we have

$$10\log\left[\frac{F(\theta = 2.046^o)}{F(\theta = 0^o)}\right]^2 = 10dB, \tag{34}$$

and this gives us $a_{effective} = 0.0521m$.

Having obtained the aperture size, we can determine calculate the aperture efficiency from

$$\eta = \frac{| < \Phi | \Psi > |^2}{< \Phi | \Phi >< \Psi | \Psi >} \tag{35}$$

where

$$< \Phi | \Psi >= \int \int \Phi \Psi^* dx dy. \tag{36}$$

Choosing Φ as a tophat with a hole in the middle, which corresponds to the antenna main dish (radius 3 m) with the subreflector blockage (radius 0.175 m), and still normalize it with respect to the incoming tophat, and choosing Ψ as the radiation pattern from the feed (plus lens) with aperture radius $a_{horn} = 0.0521m$, we obtain,

$$\eta \approx 82.7\%. \tag{37}$$

A multimode Gaussian beam calculation gives very similar results.

3.2 The Size of the Reference Holography Feed

Since the purpose of the reference receiver is to provide an amplitude and phase standard for the main holography receiver, we require that the amplitude and phase of the reference feed do not change significantly during the range of scan of the main dish. For a 128 by 128 map, with the spacing between data points about 83.7", the total angular range of scan is about $\pm 1.5^o$. We therefore require the amplitude and phase of the radiation field of the reference horn to be relatively flat within this range.

A rule of thumb for choosing the size of the reference horn is that it should be smaller or equal to the size of the resolution element on the aperture plane. For a 128 by 128 map, and for an aperture map of size 8 m by 8 m, this gives the size of the horn about 6 cm, or the radius of the horn about 3.0 cm. To leave enough margin, we have chosen the (equivalent) radius of the reference horn to be 1.5 cm. To confirm this

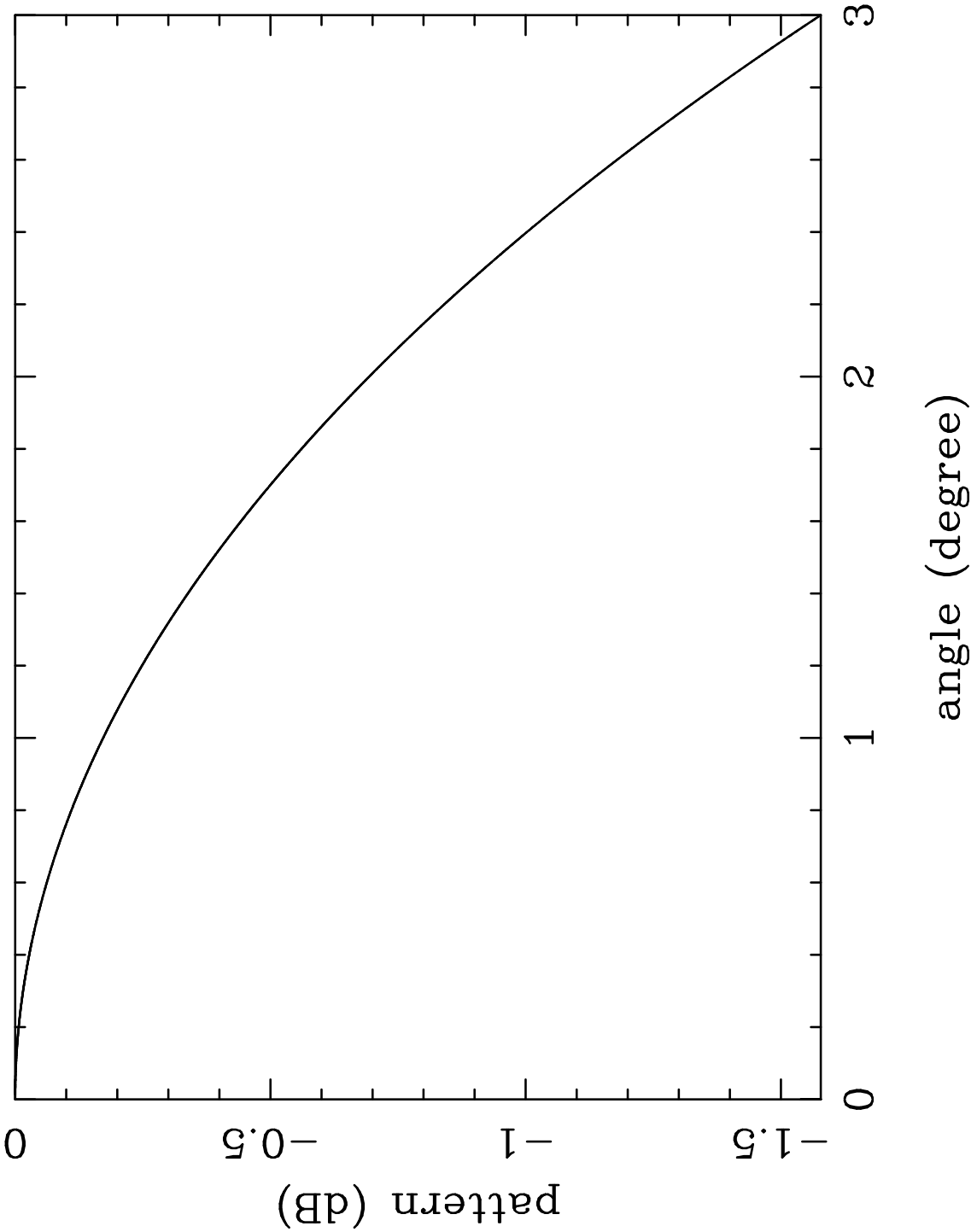

Figure 7: Radiation pattern of the reference horn with phase corrector lens

estimate, in Figure 7 we have plotted the calculated far-field pattern of the reference feed. We can see that the amplitude distribution is reasonably flat, especially within the central 1.5^o. If we do reference the main receiver amplitude with respect to the reference receiver amplitude, even this small (but known) amplitude change can be taken out[3]. The phase pattern should be flat for a horn with a phase-corrector lens, if the transmitter is in its far field.

4 Location of the Main Holography Receiver

In the last section, we have calculated the size of the main holography feed for a desired edge taper using far-field calculations. Since the resulting horn size is rather large, it turns out that the subreflector is not yet at the far field of the main feed. This introduces mainly two deviations from the far field result, which need to be compensated for:

1. The radius of curvature of the wavefront of the feed at a distance from the Cassegrain focus to the subreflector is not equal to that distance. Therefore, we need to match the wavefront curvature the best we can, which means that we need to place the feed at a location different from the Cassegrain focus, and then estimate the residual error that such an operation still could not fit perfectly the wavefront at the subreflector, since the wavefront is not perfectly spherical.

2. At the selected location which best fit the wavefront curvature, the resulting edge taper as well as the aperture efficiency are different from their corresponding values obtained from far-field calculations. This second effect will only be estimated but not corrected, since a small change in edge taper and aperture efficiency does not influence the quality of the holography experiment.

We calculate the near-field effect using the multi-mode Gaussian beam approach, following that described in Lesurf (1990). In cylindrical coordinates, the solution to the scalar wave equation

[3]There remains the possibility that we will not calibrate the amplitude obtained from the main receiver against the amplitude of the reference horn, but will go to boresight periodically to get the reference amplitude.

$$\nabla^2\psi + k^2\psi = 0 \tag{38}$$

under the assumption of paraxial beam can be represented as the superposition of modes each in the form of a Gaussian multiplied by a generalized Laguerre polynomial. If we further assume cylindrical symmetry in these solutions, the pth mode can be written as

$$\psi_p = \frac{1}{\omega} L_p\left(\frac{2r^2}{\omega^2}\right) exp[-j(kz - 2\pi ft)] exp\{j\Phi_p - r^2\left[\left(\frac{1}{\omega}\right)^2 + \frac{jk}{2R}\right]\} \tag{39}$$

where

$$\Phi_p = (2p+1)\tan^{-1}(\frac{\lambda z}{\pi\omega_0^2}), \tag{40}$$

where ω_0 is the beam waist size at $z = 0$ and

$$\omega^2 = \omega_0^2\left[1 + \left(\frac{\lambda z}{\pi\omega_0^2}\right)^2\right] \tag{41}$$

is the waist size at z, and

$$R = z\left[1 + \left(\frac{\pi\omega_0^2}{\lambda z}\right)^2\right] \tag{42}$$

is the wave-front curvature of the fundamental mode (p=0) at z. The expression and recurrence relation for the Laguerre polynomial $L_p(t)$ are

$$L_0(t) = \sqrt{\frac{2}{\pi}} \tag{43}$$

$$L_1(t) = \sqrt{\frac{2}{\pi}}(1-t) \tag{44}$$

$$L_2(t) = \sqrt{\frac{2}{\pi}}(\frac{t^2}{2} - 2t + 1) \tag{45}$$

$$\cdots$$

$$L_n + 1 = 2L_n - L_{n-1} - [(1+t)L_n - L_{n-1}]/(n+1). \tag{46}$$

The Gauss-Laguerre modes ψ_p satisfy the orthogonality and normalization condition

$$< \psi_p | \psi_{p'} >= \begin{array}{ll} 1 & p = p' \\ 0 & p \neq p' \end{array} \qquad (47)$$

Having obtained the Gauss-Laguerre mode expansion for the field in the feed (plus lens) aperture, which we take to be the beam waist, the field solution at any point along the beam propagating direction can be written as the superposition of these same modes propagated according to the expressions give above. We can already see from these expressions that if $z < \infty$, the fundamental mode radius of curvature at a distance z from the feed is larger than z. This means that we can move the feed closer to the subreflector from the Cassegrain focus. However, the fundamental mode is not the only component that determines the wavefront phase distribution. The anomalous phase Φ also contributes to the overall wavefront phase. When the two contributions are added together, we obtain an overall phase distribution, shown in Figure 8 for the actual location of the holography feed, which has the horn aperture about $4.642m$ from the vertex of the subreflector[4]. This phase distribution is best fitted by a spherical wave of $R = 4.77m$, which gives a residual error distribution shown in Figure 9, with maximum residual error of $1.8 \cdot 10^{-2} rad$, or 1.03^o.

Since the nominal Cassegrain focus is $z = 4.898m$ away from the edge of the subreflector, or 4.847 from the vertex of the subreflector, the equivalent forward feed movement is $4.847 - 4.77 = 0.077m$, which can be compensated by a corresponding subreflector movement of $77/800 = 0.1mm$. The residual error due to that defocus cannot be fitted by a second order function (Appendix II) is about 0.4^o.

5 Location of the Reference Receiver and the Determination of the Phase Reference Plane

When the antenna dish pivots about the intersecting points between the azimuth and elevation axis O' (Figure 10), there is a difference in the wavefront arrival phase for

[4]Note that this location, z = 4.642 m from the vertex of the subreflector, is not the optimum location in terms of minimum residual phase error. This location is chosen mainly because it is the only accessible location for the holography main receiver, which is sandwiched between the weather window in front and mirror No.4 behind.

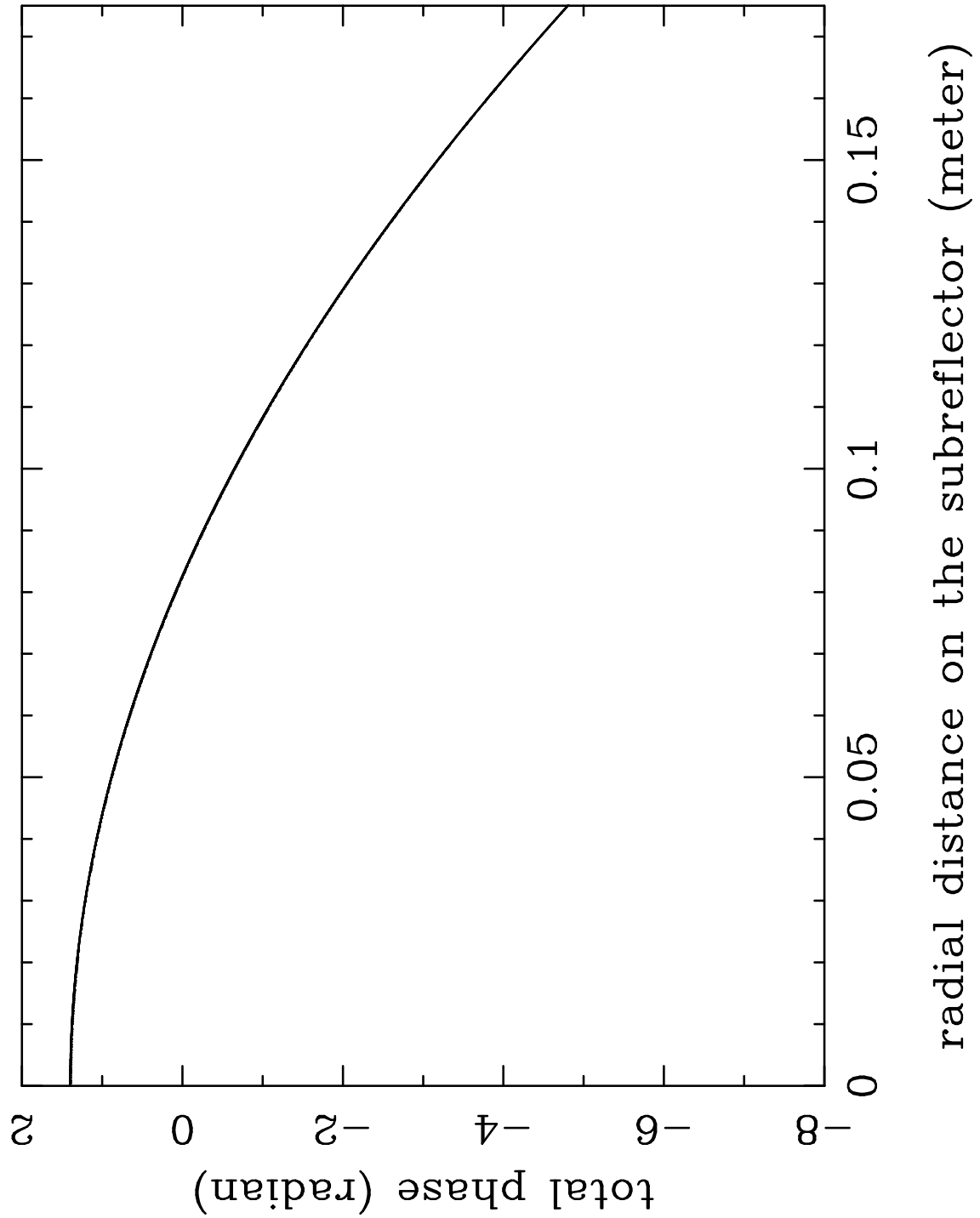

Figure 8: Wavefront phase at the edge of the subreflector for a feed located 4.642 m behind

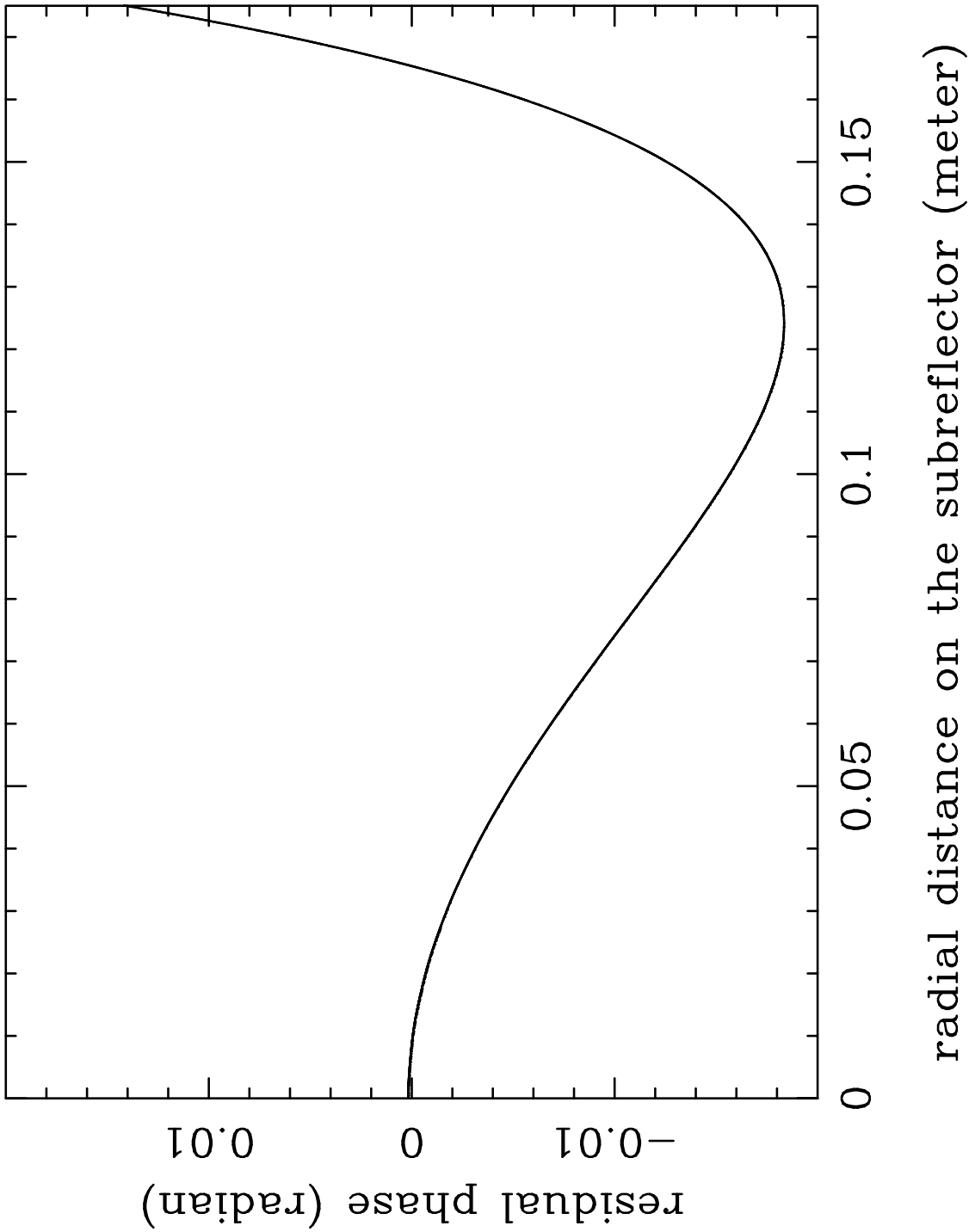

Figure 9: Residual phase after taking out a spherical wavefront of R = 4.77 m

the different pivoting angles. Since the phase reference receiver is mounted on the back of the chopping secondary control housing, both the wavefront arriving at the main antenna dish and at the reference receiver need to be corrected for this wavefront arrival phase difference for azimuth and elevation angles different from boresight.

Using the notations indicated in Figure 10, we have that the correct phase at each pivoting angle θ is related to the main and reference receiver recorded phases, as well as the correction terms through

$$\begin{aligned} phase(\theta) &= [\text{recorded\_phase}(O) + r(1-\cos\theta)] - [\text{recorded\_phase}(O_1) + R(1-\cos\theta)] \\ &= [\text{recorded\_phase}(O) - \text{recorded\_phase}(O_1)] + (r-R)(1-\cos\theta). \end{aligned} \tag{48}$$

We therefore need to know the distance from the pivoting point O' to the phase reference plane of the main reflector (usually chosen to be in the middle of the reflector), and to the phase reference plane of the reference receiver (chosen to be half-way into the thickness of the aperture lens). We now estimate what accuracy we need to estimate these two distances.

For a maximum pivoting angle of 1.5^o (128 by 128 map), and for a surface error of 5 micron, or pathlength error of 10 micron, we have

$$(r-R)_{(\text{maximum\_error})} = 30mm, \tag{49}$$

i.e. each quantity could have a maximum measurement error of 15 mm.

In practice, we sometimes want to calculate the phase distribution on a plane which is different from our initial phase reference plane. For example, if we want to move the reference plane back by an amount $z_0 < 0$, we could accomplish this by multiplying the measure far-field pattern $F_1(u,v)$ (after applying the original phase correction [48]. Note that without doing this initial correction, the effective phase reference is at the horn aperture of the phase-reference receiver) with a factor $e^{-jkz_0\cos\theta}$, i.e.

$$F(u,v) = F_1(u,v)e^{-jkz_0\cos\theta}, \tag{50}$$

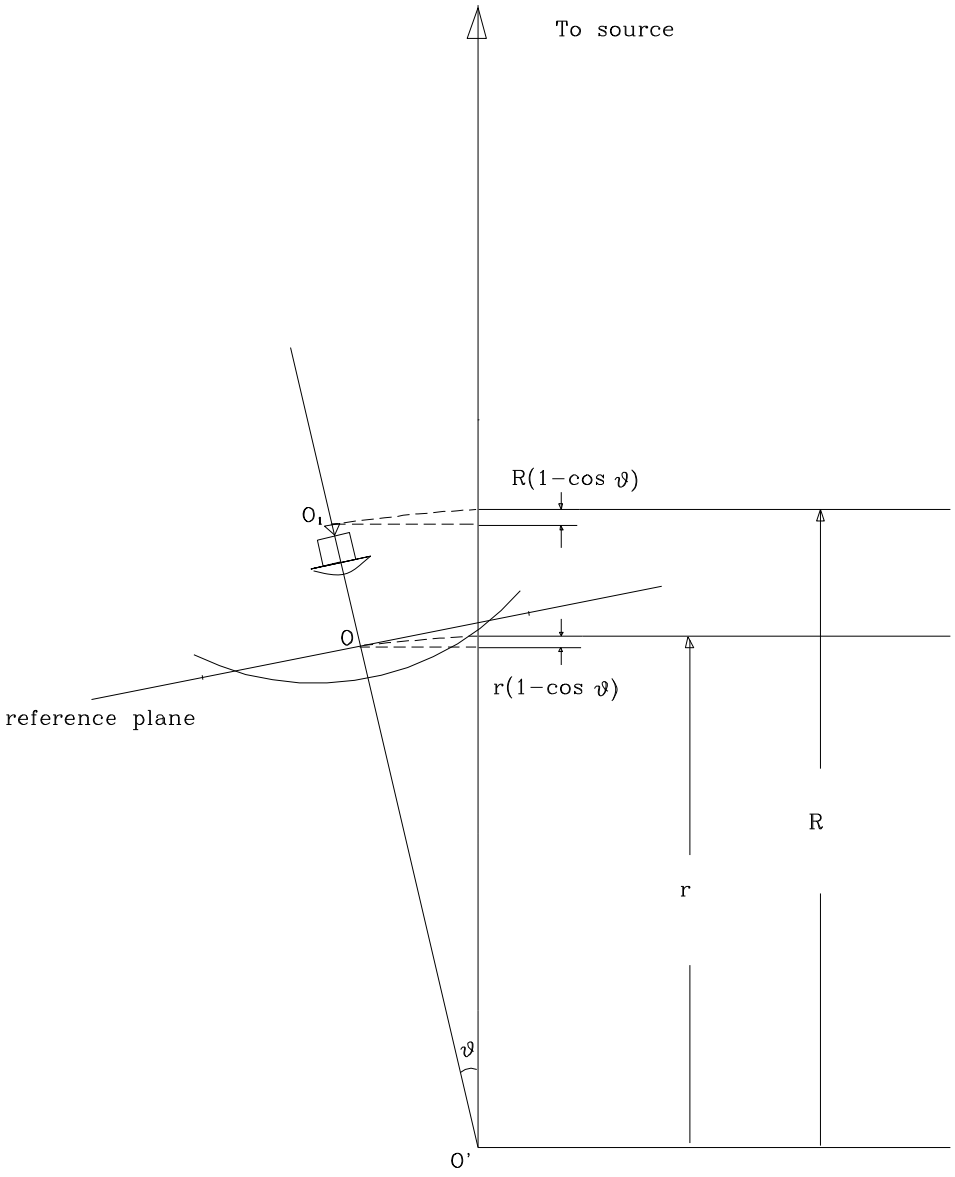

Figure 10: Determining the phase reference plane

before performing the Fourier transform to obtain the aperture field.

For the actual geometry of the SMA antennas and the wavelength we are using, the depth of the antenna surface, about 1 m, is smaller than the Fresnel distance $0.1 \cdot L^2/\lambda$ for most of the panels. So we probably do not need to change reference plane during the calculation of phase error for different rings of panels. We will experiment with the actual data taken to make sure that the difference between these two approaches are not significant.

6 Location of the Transmitter, Near-Field Effect

At the Haystack site, the beacon transmitter for the holography experiment will be mounted on the Lowell Tower which is about 250 meters away from the antenna pads. On the other hand, the far-field distance is $2D^2/\lambda \approx 22000$ meters. Therefore we need to look into the near-field effect this introduces and the ways to correct for it.

Referring to Figure 11a, we know that the radiated field $F(s,t)$, which is measured on a spherical surface with respect to the antenna pivoting point, is related to the antenna aperture field $E(x,y)$ by the Fresnel-Kirchhoff integral

$$F(s,t) \propto \int_{aperture} \frac{(1+\cos\theta)}{2} \frac{e^{-jkd}}{d} E(x,y) dx dy. \tag{51}$$

Following Hills (1986), we make the following approximations:

1. $\cos\theta \approx 1$.
2. $1/d \approx 1/R$ except in the expression for the phase.
3. For the phase term, $d^2 = R^2 - s^2 + (s-x)^2$, therefore $d \approx \sqrt{(R^2 - 2sx + x^2)} \approx R - \frac{sx}{R} + \frac{x^2}{2R} + \frac{1}{8}\frac{(2sx-x^2)^2}{R^3}$.

Therefore to second order

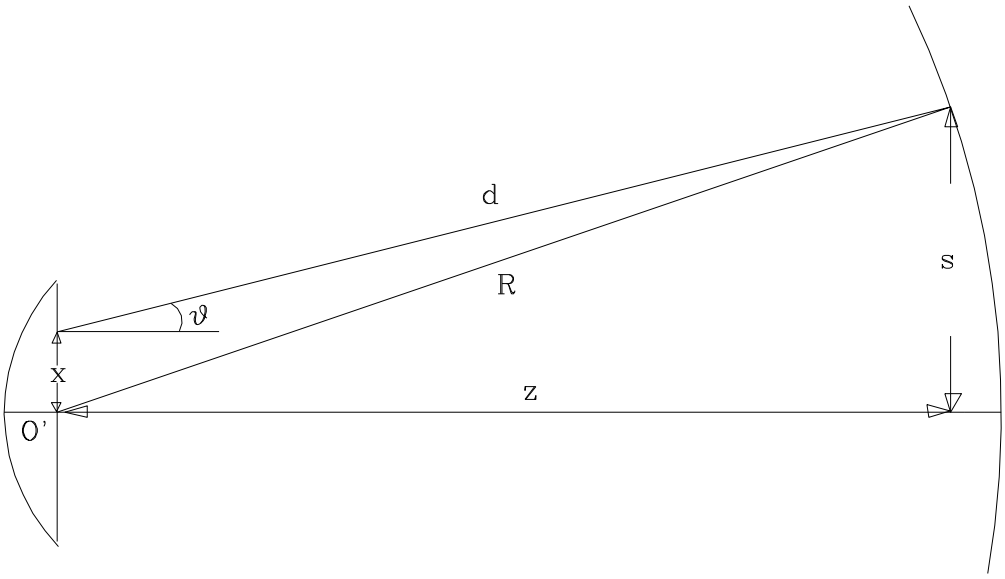

(a) Fresnel–Kirchhoff's integral relation

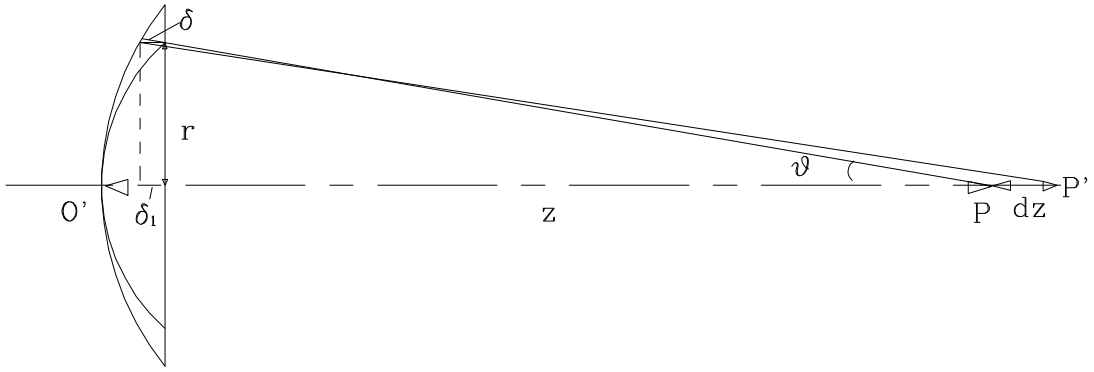

(b) Derivation of the accuracy needed for the distance from the antenna pivoting point to the transmitter

Figure 11: Calculation of the near-field effect

$$F(s,t) \propto \int_{aperture} e^{jk\frac{sx+ty}{R}} e^{-jk\frac{x^2+y^2}{2R}} E(x,y)dxdy \tag{52}$$

Let $x_i = i\frac{D'}{N}$, $y_j = j\frac{D'}{N}$, $\frac{s_m}{R} = m\frac{\lambda}{D'}$, $\frac{t_n}{R} = n\frac{\lambda}{D'}$, where D' is the size of the aperture map (could choose to be larger than the primary mirror diameter), and N is the total number of data points in one dimension (N is always chosen to be even), using also that $k = \frac{2\pi}{\lambda}$, we have

$$F(s_m,t_n) \approx \sum_{i=-N/2}^{N/2-1} \sum_{j=-N/2}^{N/2-1} e^{j\frac{2\pi}{N}(im+jn)} \cdot e^{-jk\frac{x_i^2+y_j^2}{2R}} E(x_i,y_j) \tag{53}$$

$$\propto \mathrm{DFT}^{-1}[E(x_i,y_j)e^{-jk\frac{x_i^2+y_j^2}{2R}}]$$

Since the spherical wave term depends only on the aperture field parameters but not on the parameters of the radiation plane, we can invert this and write

$$E(x_i,y_i) = \mathrm{DFT}[F(s_m,t_n)] \cdot e^{jk\frac{x_i^2+y_j^2}{2R}}, \tag{54}$$

i.e. the major near-field correction factor is in the form of a second-order wavefront correction for the aperture field.

To estimate the residual error after we have applied this second order correction, we take a closer look at the next order term. The next order pathlength correction term is of the form

$$\epsilon = \frac{[x^2+y^2-2(sx+ty)]^2}{8R^3} \tag{55}$$

The worst case for the above expression is when the vectors (x,y) and (s,t) are aligned opposite to each other, and for points lying on the boundary of both the aperture map and radiation pattern. In this case,

$$\epsilon = \frac{(r_{max}^2+2r_{max}u_{max})^2}{8R^3} \tag{56}$$

with $r_{max} = 3m$, $R = 250m$ and $u_{max} = R(1.5^o \cdot \pi/180) = 6.5m$ for a 128 by 128 map. Therefore we have

$$\epsilon_{max} \approx 18\mu m, \tag{57}$$

which corresponds to a surface error of 9 μm. This however is a worst-case scenario and for most of the points on the map the errors are significantly smaller than this. This is confirmed by the diffraction-integral/ back-transform calculation presented later in section 7, where we see that after a second-order near-field correction the rms phase error on the recovered aperture map is about 0.3^o for the 128 by 128 map, a level which includes both the residual phase error due to near-field effect and the effect of aliasing. The third order term cannot be completely corrected for in a direct calculation, since part of it depends on the far-field dimension as well as on the aperture dimensions. But obviously the second order near-field correction is sufficient for our purpose of achieving a surface rms of 5 μm.

In the following, we estimate the accuracy needed for determining the distance to the transmitter. Referring now to Figure 11b, we see that an error in the distance determination dz translates into an error δ in the wavefront arrival phase at a height r above the center of the main reflector. From this same figure, we see that

$$\delta = \delta_1 \cos\theta, \tag{58}$$

and where δ_1 itself can be calculated as

$$\delta_1 = (z - \sqrt{z^2 - r^2}) - [(z + dz) - \sqrt{(z + dz)^2 - r^2}] \approx -dz + \frac{dz \cdot z}{\sqrt{z^2 - r^2}}. \tag{59}$$

Therefore,

$$\delta = dz \left(\frac{z}{\sqrt{z^2 - r^2}} - 1 \right) \frac{\sqrt{z^2 - r^2}}{z} \approx \frac{1}{2} dz \frac{r^2}{z^2} \tag{60}$$

For a maximum $\delta = 10^{-5}$ (10 micron pathlength error or 5 micron surface error), at $r = 3m$ and $z = 250m$ we obtain from the above expression that the error for dz is

about 14 cm. This of course is for the edge region and the error for dz can be relaxed a little if we only seek an rms surface error of 5 microns.

Finally, we use BEAM 4 raytracer to calculate what is amount of subreflector travel required in order to focus at 250 m distance. In Figures 12, 13 and 14, we have plotted the geometric optics images at a distance 250 meters away from the antenna vertex, for subreflector (outward) movement of 3.5, 4.0, and 4.5 cm, respectively (note that the vertical and horizontal scales are not equal). We see that we obtain the tightest focus at a subreflector travel of about 4.0 cm. Therefore we have requested a spec for the chopping secondary to have a maximum travel of 4.5 cm. This allows us not only to focus the beam in the phase-coherent holography case, but also leaves enough margin to obtain a (1 wavelength) defocused maps at both sides of the focus for doing phase-retrieval holography.

We also note that in all the above cases the geometric spot size is less than 1 m in radius. Since for a 128 by 128 map we sample the beam to about 1.5^o or $6.5m$ in radius, we expect that we have covered the entire Fresnel image region so aliasing should not be a serious problem. This will be further confirmed by performing the Fresnel-Kirchhoff's integral directly, which we will do in the next section.

7 Effect of Aliasing

We investigate the effect of aliasing by performing the Fresnel-Kirchhoff integral (Figure 11a), starting from a flat circular aperture with uniform illumination which represents the main reflector of the SMA antenna, onto a spherical screen 250 meters away. We then sample the radiation pattern using the same grid as we will use for the real experiment, and then back transform the pattern using the standard FFT routine, and examine the recovered aperture amplitude and phase distributions to assess the degree of aliasing. The actual diffraction integral and FFT performed are the equivalent one-dimensional versions in order to save cpu time.

In Figure (15), we present the beam pattern of the SMA antenna at 250 m distance, calculated using the Fresnel-Kirchhoff diffraction integral. The pattern is seen to resemble the classical diffraction pattern of a circular aperture at its Fresnel zone, with alternating bright and dark rings. Figure (16) and (17) plot the recovered

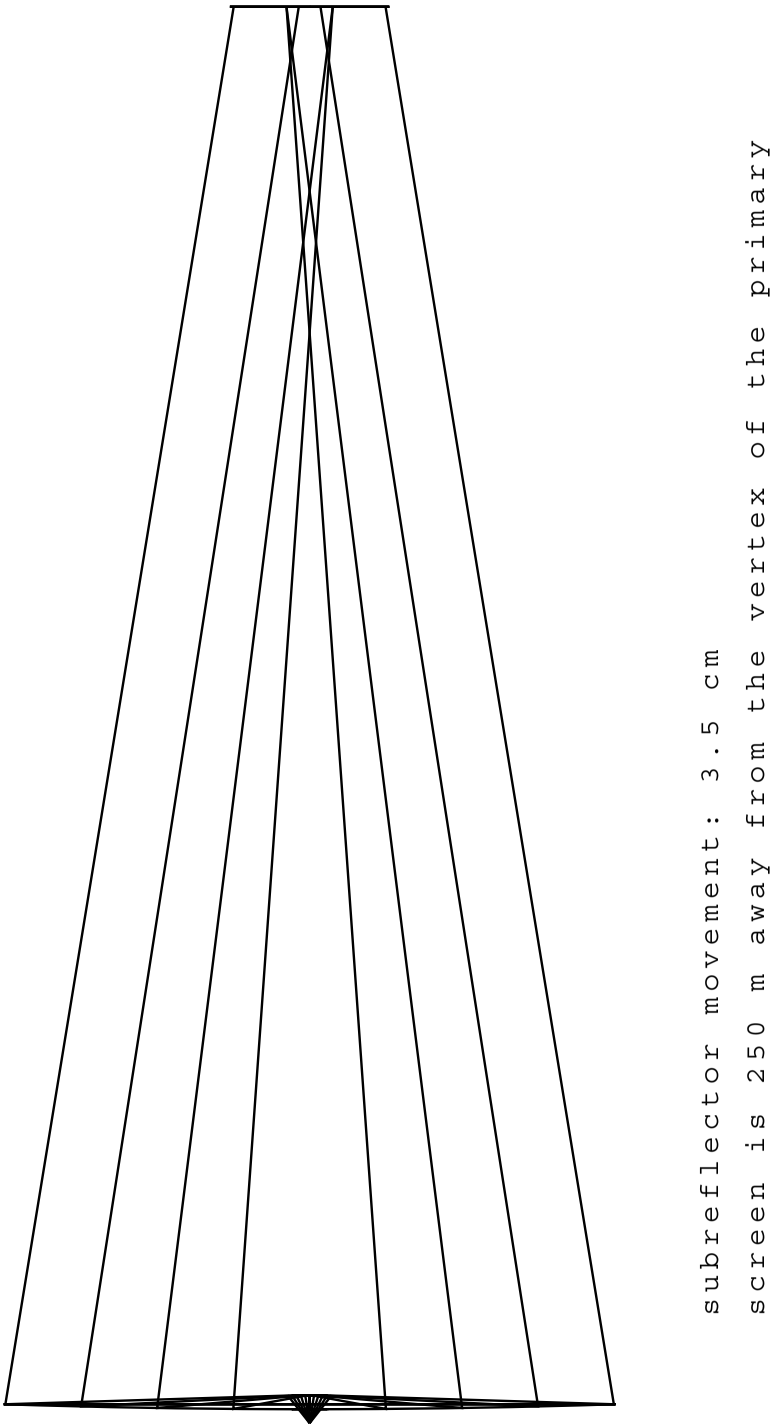

Figure 12: Ray trace result for 3.5 cm subreflector movement. Screen is at 250 m away from the vertex of the antenna

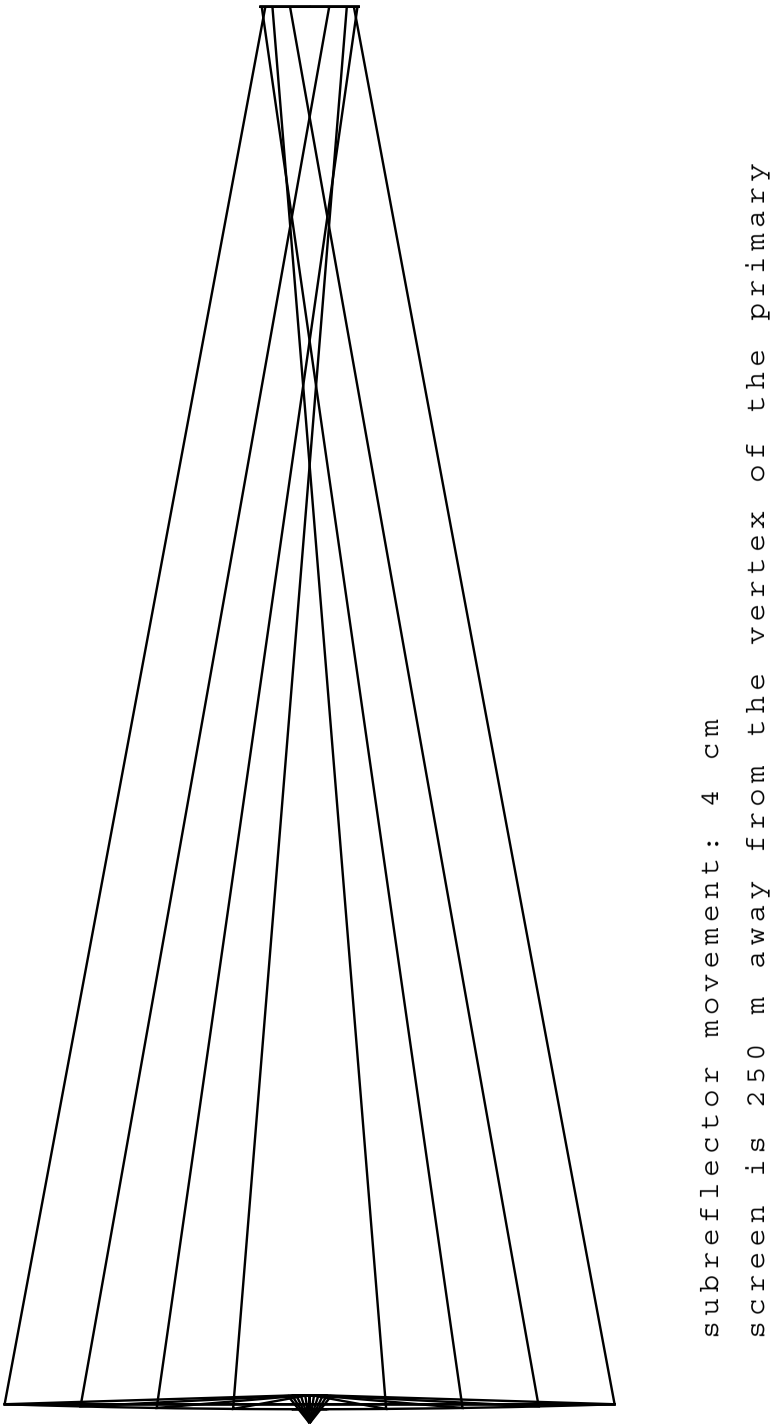

Figure 13: Ray trace result for 4.0 cm subreflector movement. Screen is at 250 m away from the vertex of the antenna

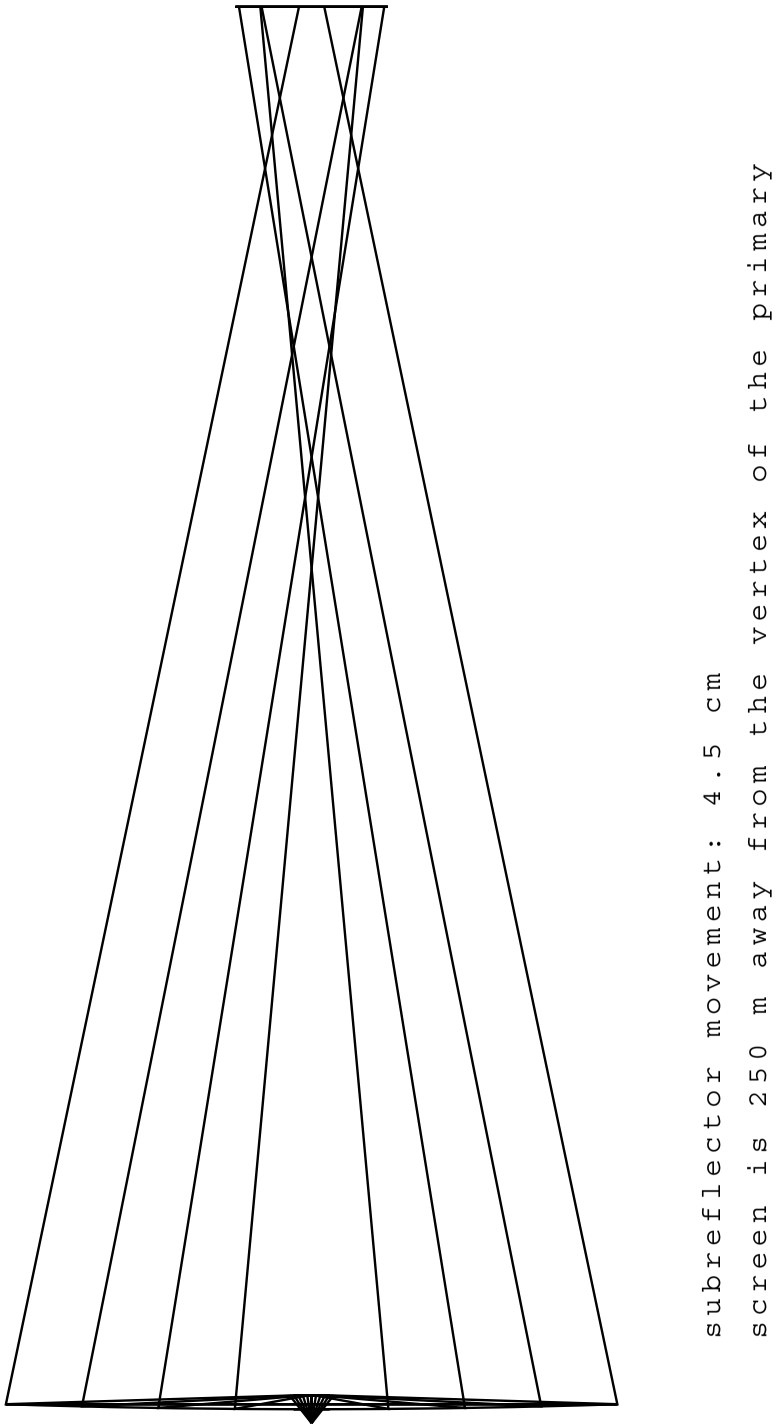

Figure 14: Ray trace result for 4.5 cm subreflector movement. Screen is at 250 m away from the vertex of the antenna

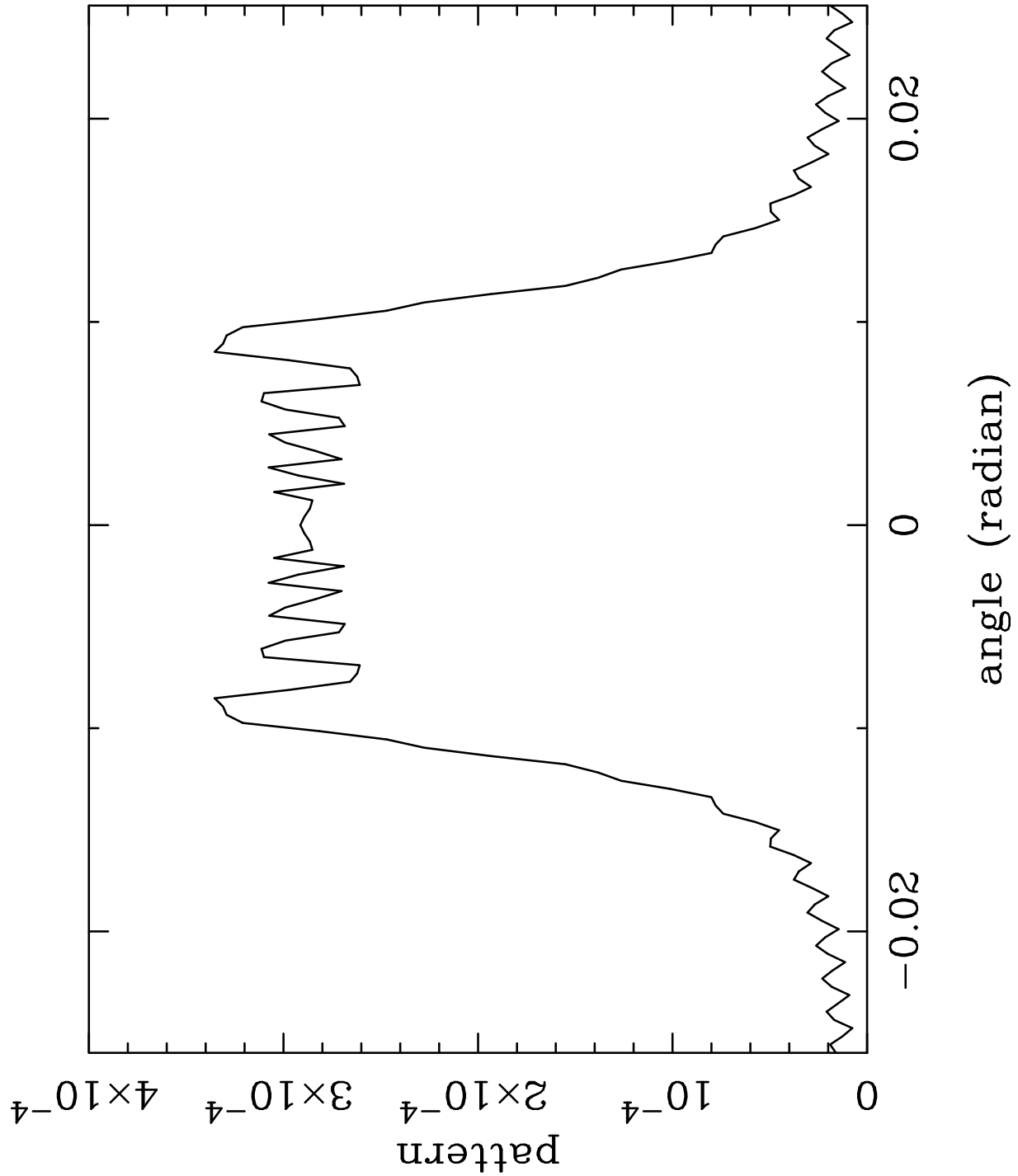

Figure 15: Amplitude pattern on a spherical screen 250 m away, no refocusing

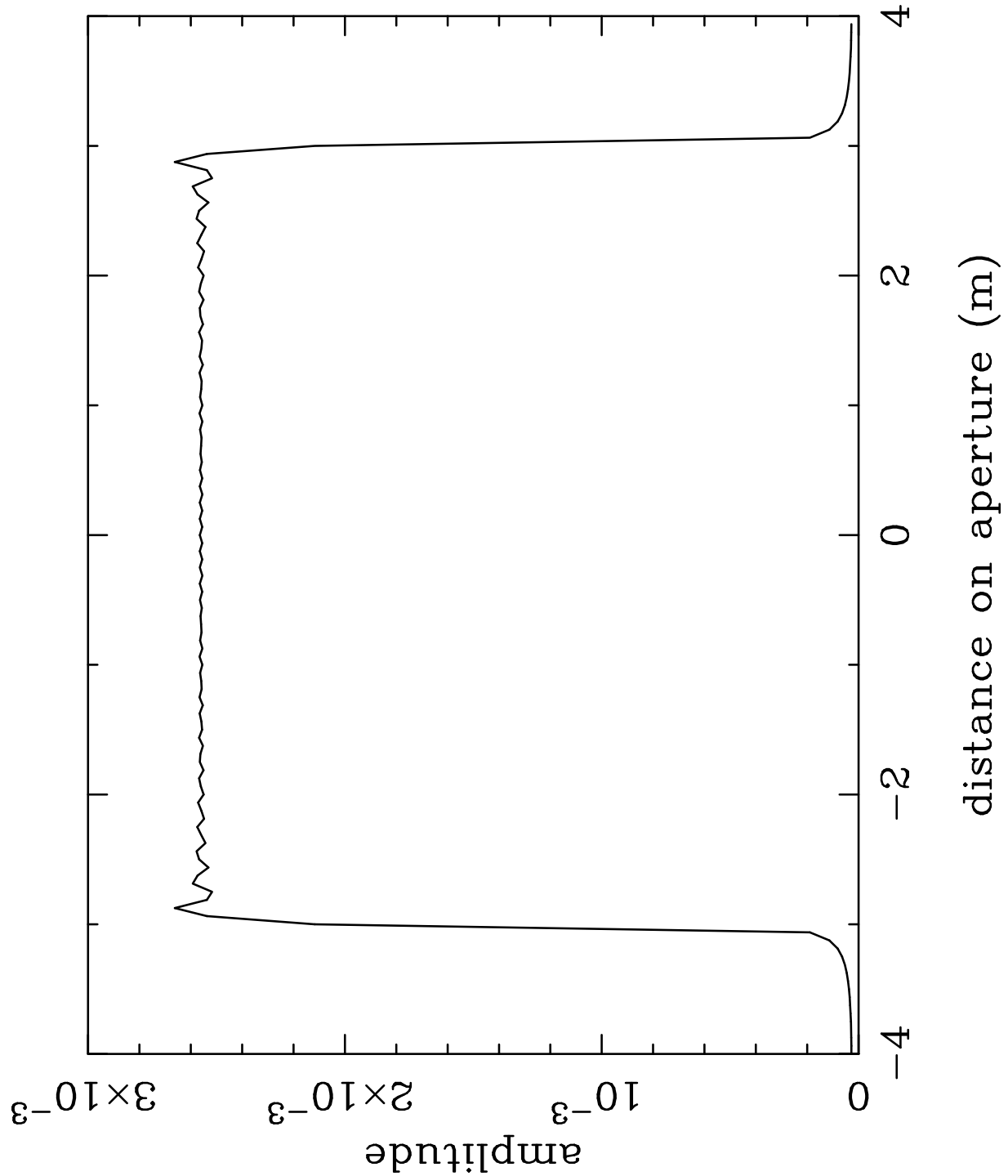

Figure 16: Recovered aperture amplitude distribution for the no-refocusing case

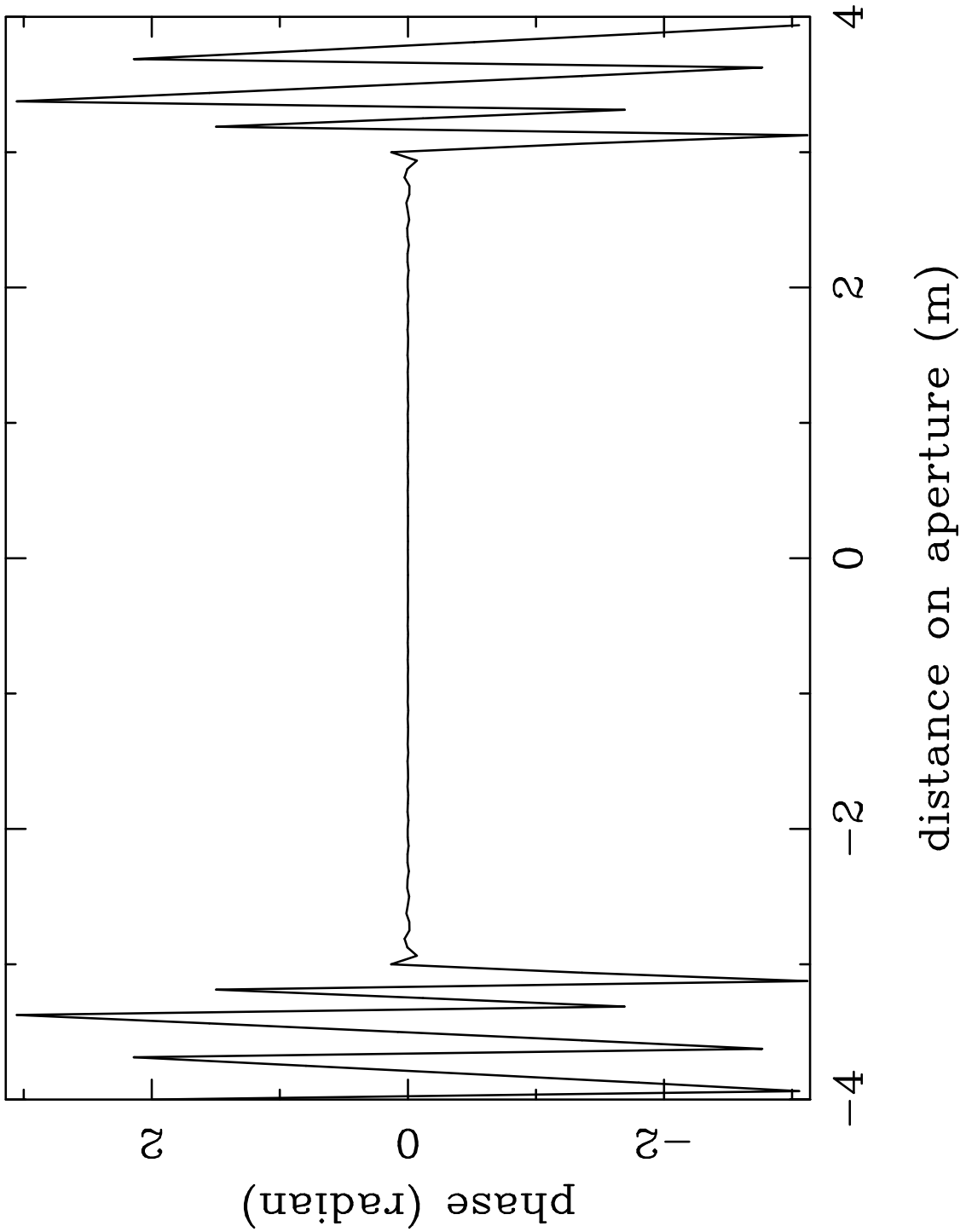

Figure 17: Recovered aperture phase distribution, with near-field correction, for the no-refocusing case

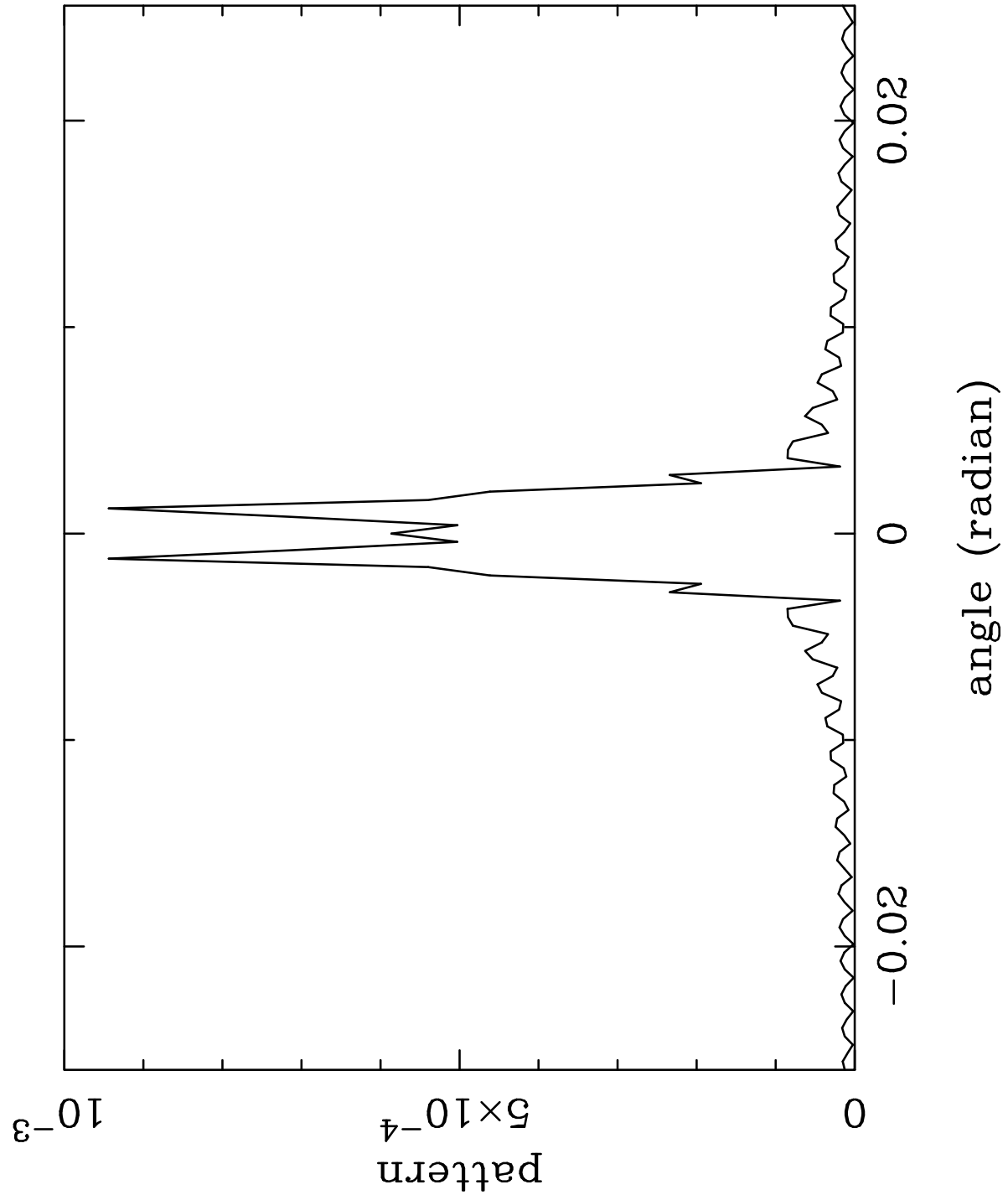

Figure 18: Amplitude pattern on a spherical screen 250 m away, 3.9 cm refocus

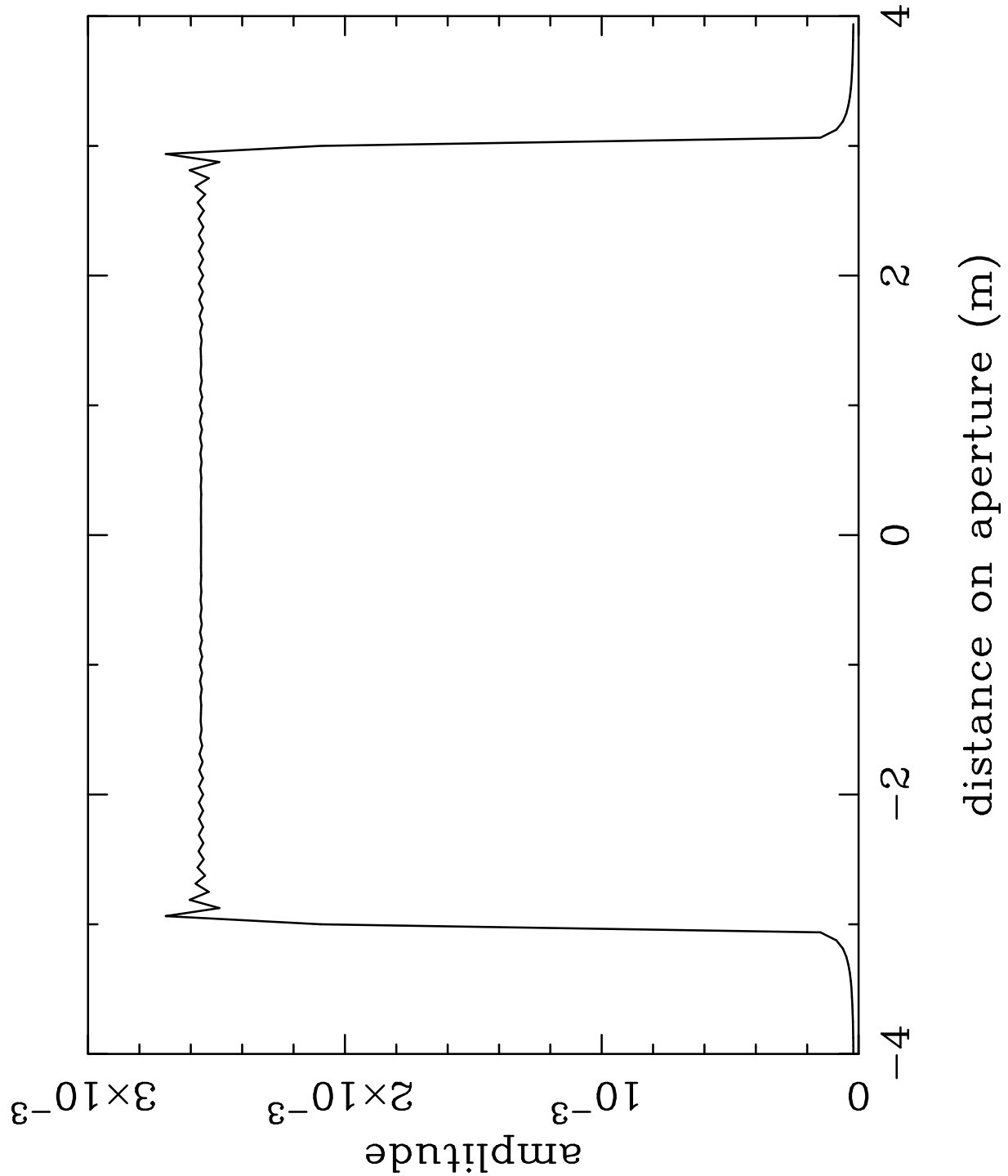

Figure 19: Recovered aperture amplitude distribution for the refocused case

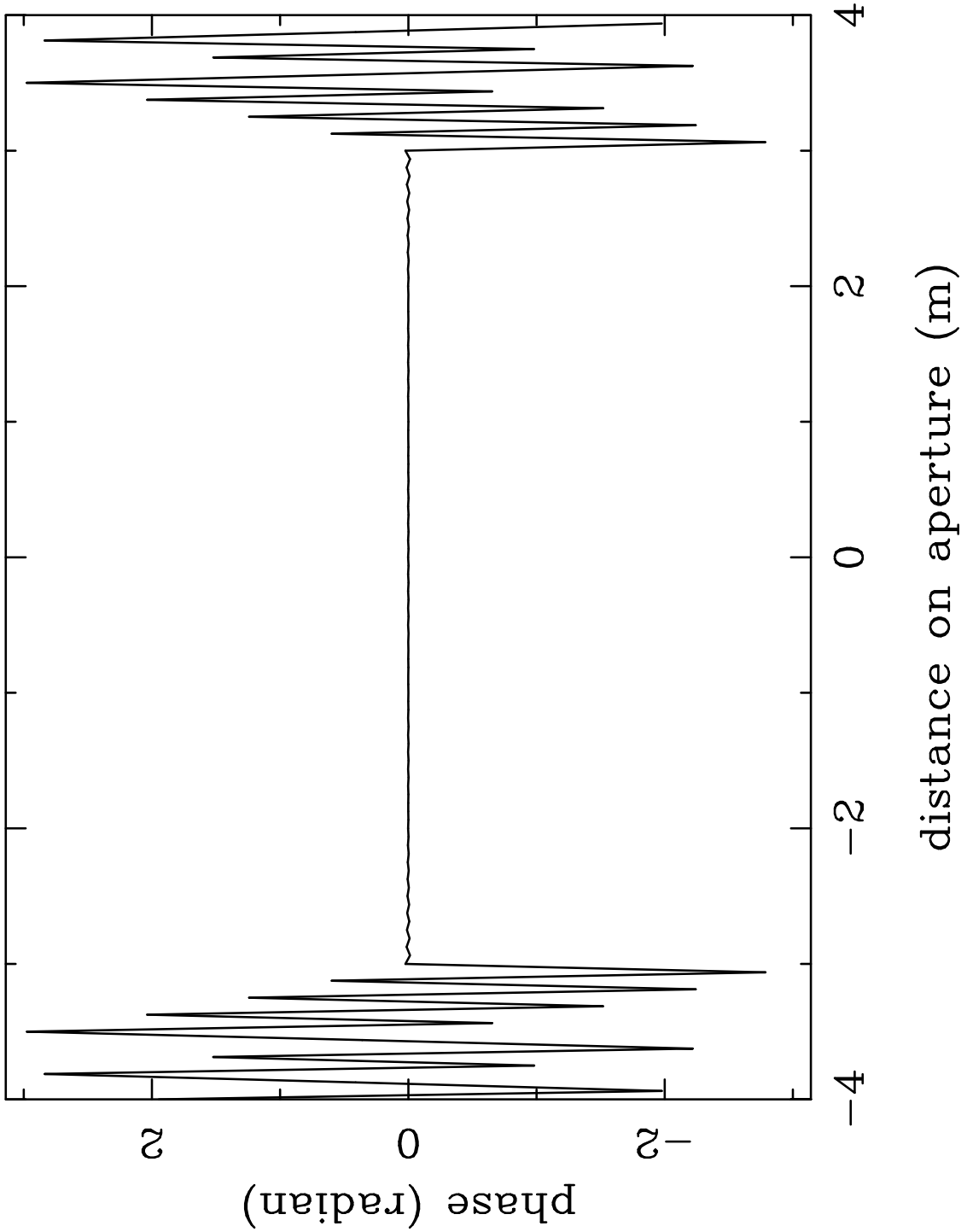

Figure 20: Recovered aperture phase distribution, with near-field correction, for the refocused case. An amount of phase due to refocus is also removed

aperture amplitude and phase distributions, obtained by performing an FFT on the Fresnel diffraction pattern followed by the second order near-field correction. It is seen that the residual errors due to aliasing are very small, for the 128 by 128 sampling we choose to use. The rms phase error in the central 3 m radius region is about 1.3^o. Note that the SMA dish surface corresponds to the central (-3m, 3m) in Figures 16 and 17.

Figures (18), (19) and (20) presents an parallel set of calculations for refocusing the telescope to the 250 meter near-field distance. The rms phase error in the central 3 m radius region in this case is about 0.3^o. The improvement on the aliasing effect is noticeable but not significant, since the error started to be small. It will only be of significance when we measure a smaller-sized beam pattern map (e.g. 64 by 64). In fact, the somewhat out-of-focused case in between of the two extremes we are showing here may be of practical advantage, since it reduces the accuracy requirement of the phase measurement on the boresight, and it also improves the dynamical range and SNR requirements for the sidelobe measurement. We will experiment with the different focus settings during the actual holography test.

Appendix I. Design of the Dielectric Lenses to Accompany the Two Receiver Feeds

The purpose of the dielectric lenses in front of the aperture of the feed horns is to change the wavefront curvature from that of approximately spherical emerging from the horn to that of a flat wavefront.

In Figure 21, considering a typical ray emerging from the phase center of the feed horn with an angle θ_i, which is also the angle of incidence onto the back plane of the lens at point P_1. The ray then emerges from P_1 with an angle θ_r inside the lens, and travels further to reach the other (curved) surface of the lens at P_2. After the second refraction at P_2, the ray should emerge to the air parallel to the axis of the horn, if the thickness d and the curvature of the lens (as represented by the set of x,y coordinates for the curved side of the lens with respect to origin O which is the center on the flat side of the lens) are properly chosen . Assuming the index of refraction of the air is n_0, and the index of refraction of the lens material is n_1, the geometry of the ray must satisfy the following relations

$$n_0 \sin\theta_i = n_1 \sin\theta_r, \tag{61}$$

$$(d-x)n_0 + \frac{x}{\cos\theta_r} n_1 + \frac{R}{\cos\theta_i} n_0 = Rn_0 + dn_1, \tag{62}$$

$$y = R\tan\theta_i + x\tan\theta_r, \tag{63}$$

where R is the distance from the vertex of the feed to origin O.

We now try to solve these three equations to derive a parametric representation of the lens profile (x,y), using the sine of the ray incident angle $\sin\theta_i$ as the parameter.

Substituting (61) into (63), we obtain

$$y = R\tan\theta_i + x\frac{\sin\theta_r}{\cos\theta_r}$$

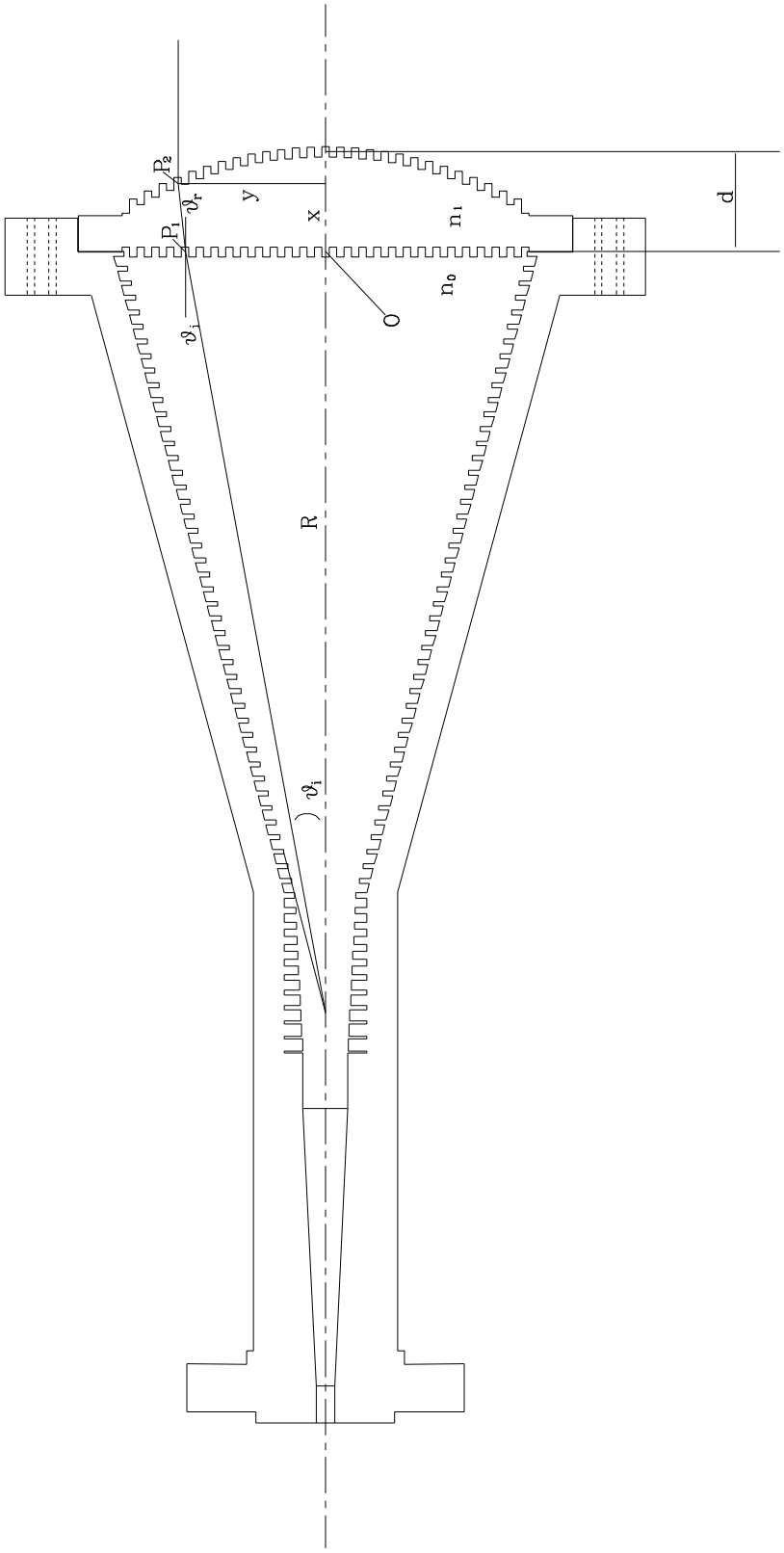

Figure 21: Schematics for the analytical ray tracing calculation

$$= R\tan\theta_i + x\frac{\frac{n_0}{n_1}\sin\theta_i}{\sqrt{1-\frac{n_0^2}{n_1^2}\sin^2\theta_i}} \tag{64}$$

Substituting (61) into (63), we obtain

$$(d-x)n_0 + \frac{x}{\sqrt{1-\frac{n_0^2}{n_1^2}\sin^2\theta_i}}n_1 + \frac{Rn_0}{\sqrt{1-\sin^2\theta_i}} = Rn_0 + dn_1 \tag{65}$$

Therefore finally, we obtained the two parametric equations for the lens profile (x,y):

$$x = \frac{Rn_0 + dn_1 - \frac{Rn_0}{\sqrt{1-\sin^2\theta_i}} - dn_0}{\frac{n_1}{\sqrt{1-\frac{n_0^2}{n_1^2}\sin^2\theta_i}} - n_0}, \tag{66}$$

and

$$y = R\frac{\sin\theta_i}{\sqrt{1-sin^2\theta_i}} + x\frac{\frac{n_0}{n_1}\sin\theta_i}{\sqrt{1-\frac{n_0^2}{n_1^2}\sin^2\theta_i}}. \tag{67}$$

The above result for the analytical ray tracing is further compared with the result of the BEAM 4 raytracer, which describe the surface of the lens by the following equation in the vertex-cartesian coordinate (Figure 22)

$$z = \frac{cr^2}{1+\sqrt{1-sc^2r^2}} + a_2r^2 + a^4r^4 + ... \tag{68}$$

The difference of the coordinates calculated by the two methods is usually less 0.01 mm.

The dimensions of the two horns and lens we used are summarized in Table 1 (the length unit is mm). We include here only the BEAM 4 calculated parameters since the analytical retracing result is represented by the parametric equations. As we have commented, the comparison of numerical values of the geometry given by the two methods shows very similar result. The shape factor used for both lenses is s=1 (spherical surface).

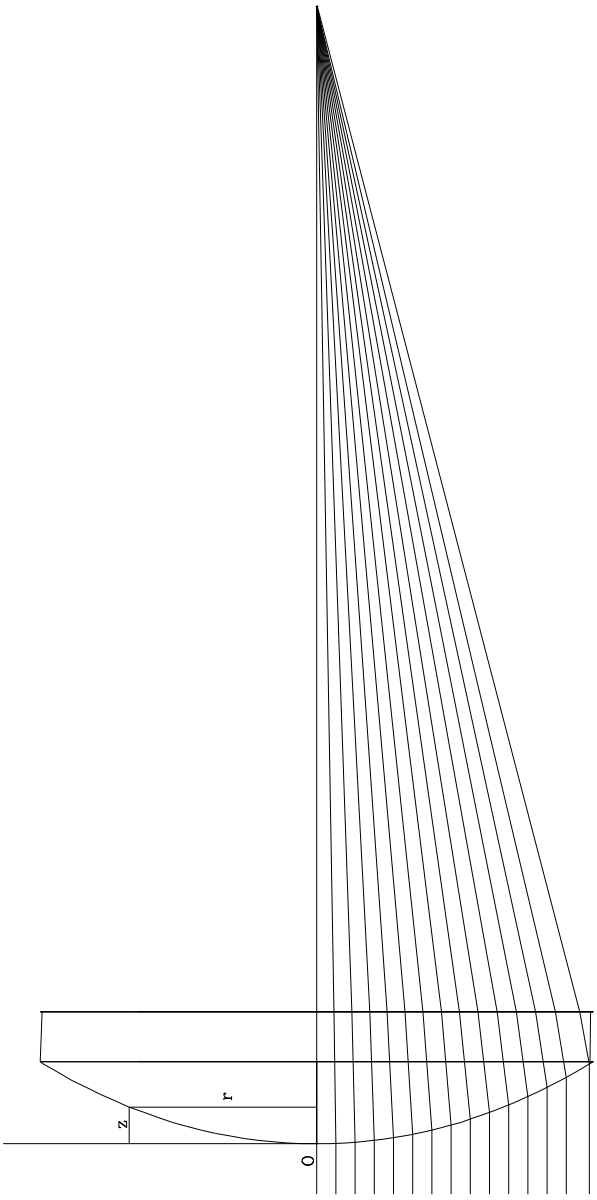

Figure 22: BEAM 4 ray tracing calculation for the lens profile

Table 1. Parameters of the Two Horns and Teflon Lenses

	R	r	d	c	a_2	a_4
Main receiver horn and lens	187	50	18.8	0.0072352	$2.071 \cdot 10^{-3}$	$3 \cdot 10^{-8}$
Reference receiver horn and lens	52.4	14	6.9	0.025383	$7.185 \cdot 10^{-3}$	$1.3 \cdot 10^{-6}$

Note that the horn dimension R and r are chosen to be 4% smaller than that given by the optics calculation, since the beam expands by approximately this amount inside the thick lens before forming the flat-wavefront image.

We now calculate the grove dimensions for anti-reflection coating the lens surface. The thickness of the AR coating layer is (Lesurf 1990, p.21)

$$t = \frac{\lambda_0}{4\sqrt{n_1}}, \tag{69}$$

where λ_0 is the free-space wavelength of the frequency range we are using. This gives $t \approx 0.686mm$ for the 90 GHz band.

The pitch of the grooves should be at least as fine as

$$p = \frac{\lambda_0}{2n_1} \tag{70}$$

which gives $p \approx 1.016$. Note that this is a rule-of-thumb which seem to work well in practice. The pitch given in Lesurf (1990) is smaller than we used here. We have also chosen to used the simple equal groove-width / ridge-width scheme, which also seems to work quite adequately in practice.

Appendix II. Pathlength Errors due to Subreflector and Feed Movement

Following Ruze (1969), we know that the pathlength error distribution on the primary mirror due to a small Δy axial movement of the feed is

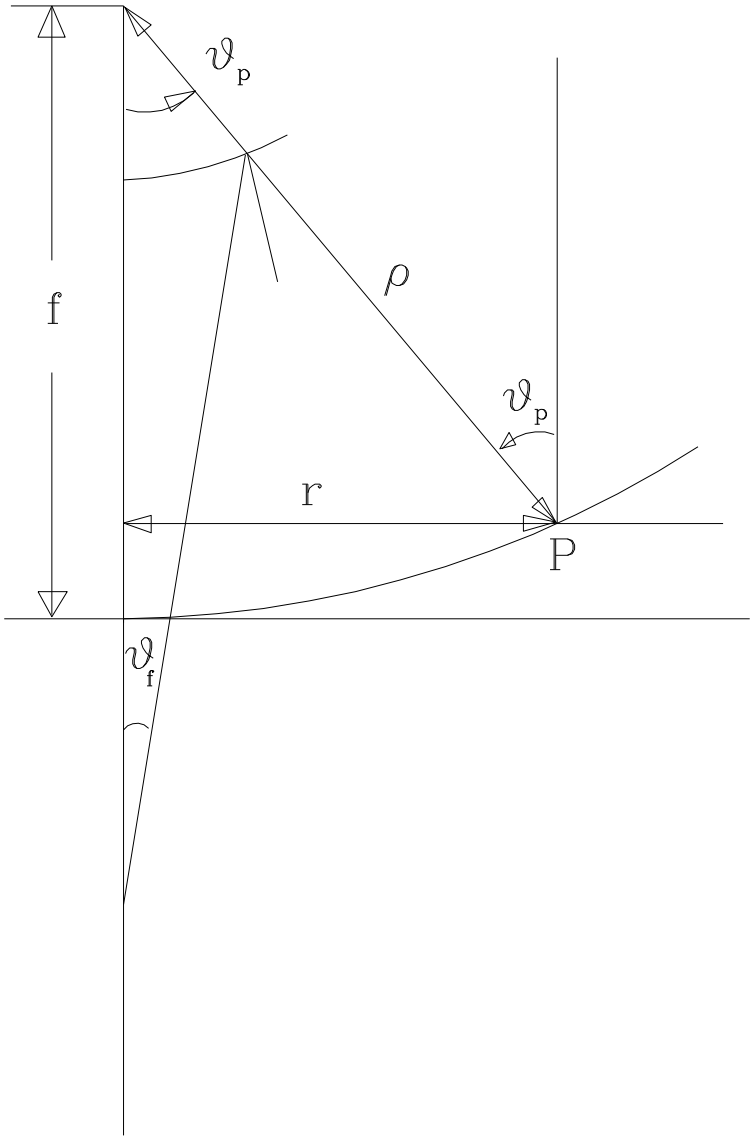

Figure 23: Cassegrain geometry

$$l_f(P) = \Delta y[1 - \cos\theta_f] \tag{71}$$

where θ_f is the angle from the location of the feed to a point on the subreflector which would be mapped onto the relevant point on the primary reflector (Figure 23).

On the other hand, the pathlength error due to a small Δy axial movement of the subreflector is

$$l_p(P) = \Delta y[(1 - \cos\theta_p) + (1 - \cos\theta_f)], \tag{72}$$

where θ_f is defined as before, and θ_p is angle made by the line connecting the prime focus to the relevant point on the primary surface.

For the SMA geometry, $(\theta_p)_{max} = 61.525^o$, and $(\theta_f)_{max} = 2.046^o$. Due to the smallness of (θ_f), the phase error distribution due to the feed movement is almost identical to a second order (r^2) function. On the other hand, the phase error due to the secondary mirror movement is more poorly approximated by a second order function. In Figure 24 and Figure 25, we plot the phase error distribution with respect to the primary radius, for 1 mm movement of the feed and the subreflector, respectively. Careful comparison shows that if we adjust the scale of the curves so that the two curves are aligned in both ends, the maximum difference of the two curves (which happens near the middle of the curves) is about 1/15 of the maximum value of the phase error. This gives us some idea of how much error it will introduce if we try to fit defocus error by a second order function (which we won't do in our software due to the large error this introduces), and how much a dislocation of the feed cannot be completely compensated for by the movement of the subreflector.

Acknowledgement

I thank Drs. Richard Hills, Colin Masson and Scott Paine for many helpful discussions.

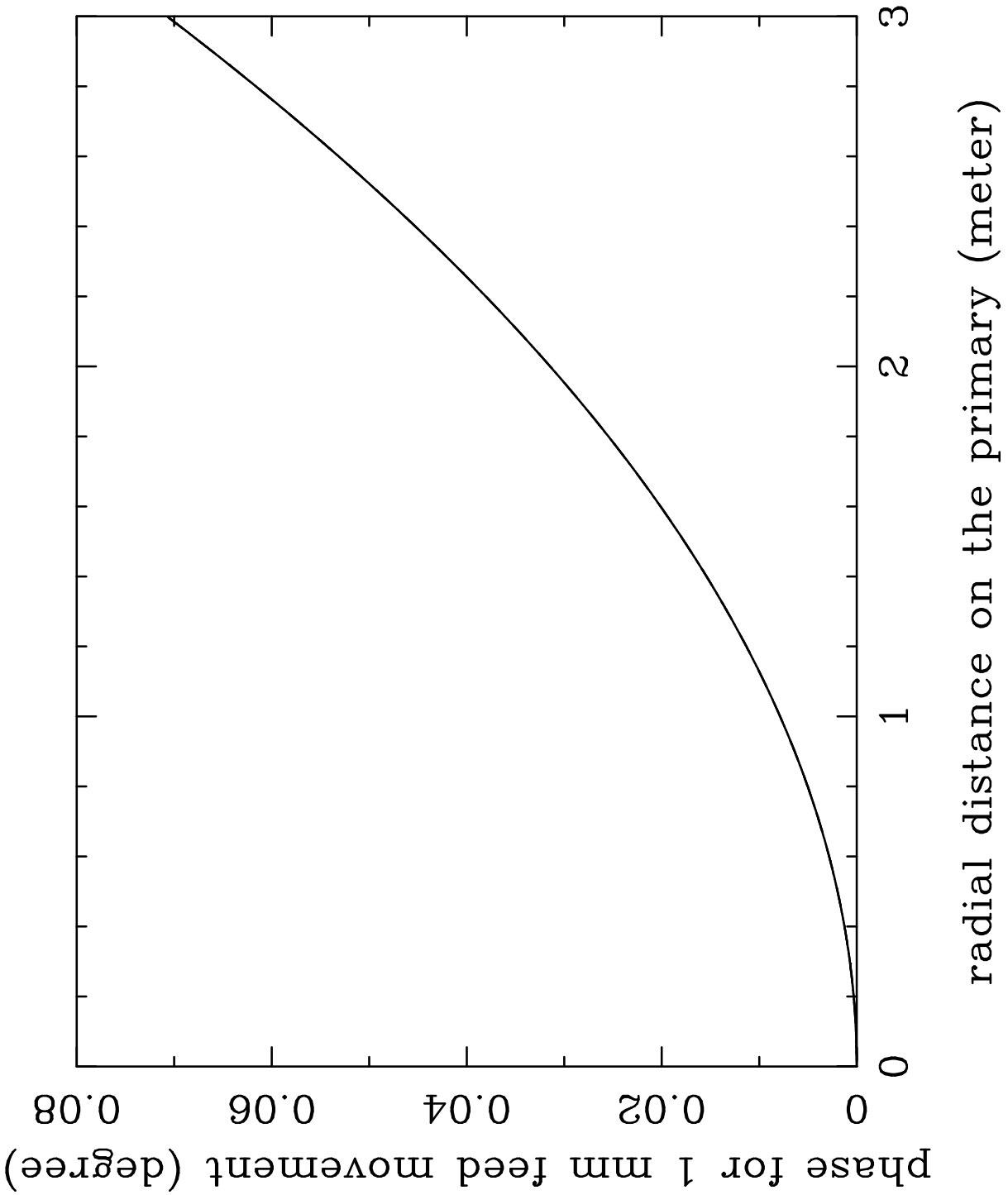

Figure 24: Phase on the primary mirror due to 1 mm feed movement

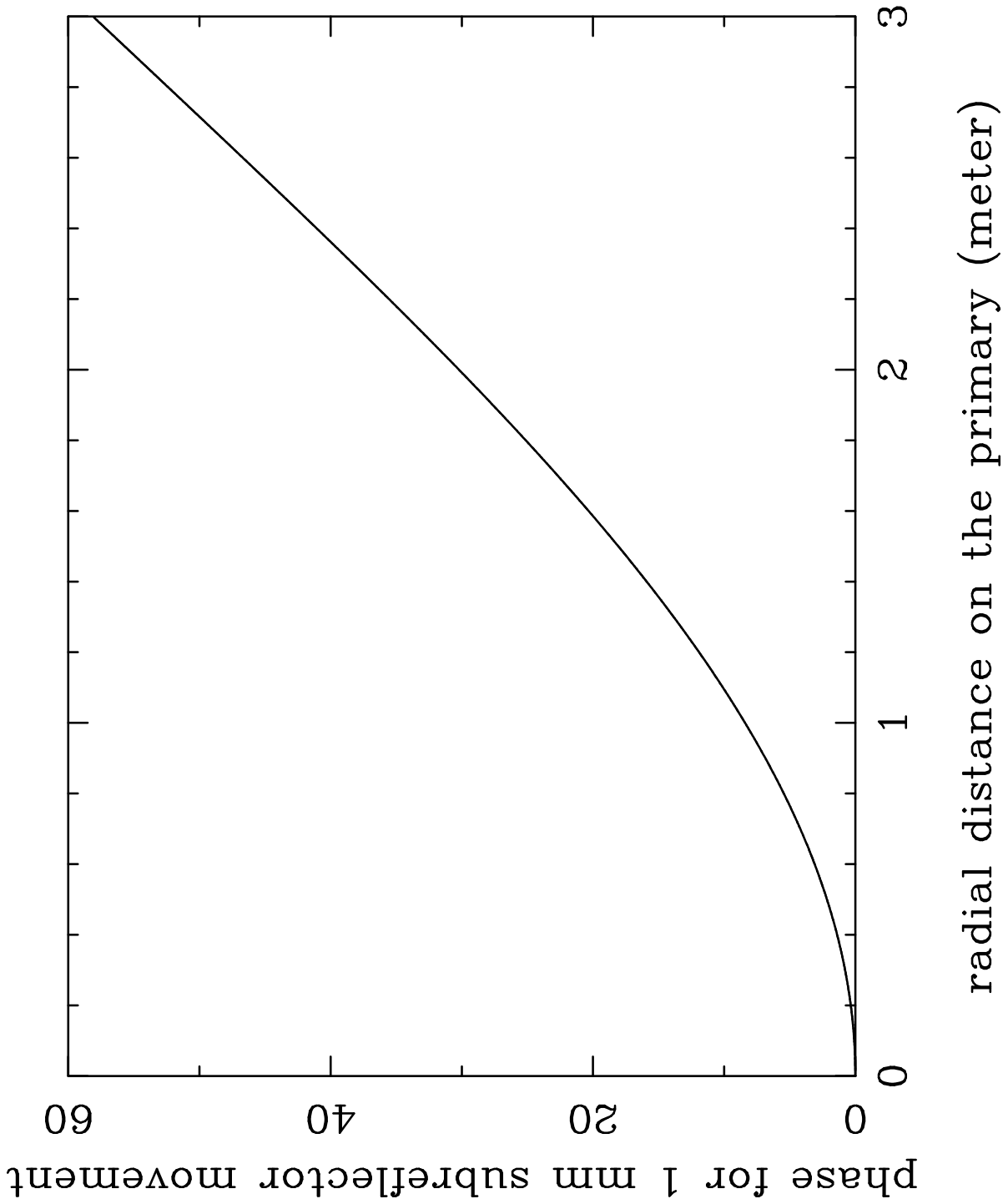

Figure 25: Phase (in degrees) on the primary mirror due to 1 mm subreflector movement

References

Dragone, 1977, "Reflection, transmission, and mode conversion in a corrugated feed," Bell Syst. Tech. J., p. 835-867

Hills, R. 1986, Memo ASR/MT/T/1015

Lesurf, J. 1990, "Millimeter-wave optics, devices and systems," (Bristol: Adam Hilger)

Rahmat-Samii, Y. 1984, "Surface diagnosis of large reflector antennas using microwave holographic metrology: An iterative approach," Radio Science, Vol.19, No.5, p. 1205-1217

Ruze, J. 1969, "Small Displacements in Parabolic Reflectors," Research Report, MIT Lincoln Laboratory

Zhang, X. 1993, "Design of Conical Corrugated Feed Horns for Wide-Band High-Frequency Applications," IEEE Trans. Microwave Theory Tech., Vol 41, No 8, p.1263-1274

Zhang, X., Levine, M., Bratko, P., Test, J., Papa, C. and Masson, C. "Planned Panel Alignment Procedure for the SMA Antennas Using the Microwave Holography Technique,", SMA technical memo, No. 85